CONTENTS

SUMMARY	1	1/A5
INTRODUCTION	1	1/A5
TEST FACILITY	2	1/A6
TEST SPECIMENS	3	1/A7
INSTRUMENTATION	4	1/A8
RESULTS AND DISCUSSION	5	1/A9
Assessment of Structural Damage	5	1/A9
Time Histories of Floor-Beam Normal Accelerations	7	1/A11
Time Histories of Floor-Beam Longitudinal Accelerations	9	1/A13
Profiles of Floor-Beam Maximum Peak-to-Peak Normal and Longitudinal Accelerations	10	1/A14
Accelerations on Cabin Seats and Occupants	11	1/B1
SUMMARY OF RESULTS	12	1/B2
REFERENCES	14	1/B4
TABLE	15	1/B5
FIGURES	16	1/B6
APPENDIX - ACCELEROMETER DATA	46	1/D8

NASA Technical Paper 1210

Light Airplane Crash Tests at Three Flight-Path Angles

Claude B. Castle and Emilio Alfaro-Bou

JUNE 1978

NASA

NASA Technical Paper 1210

Light Airplane Crash Tests at Three Flight-Path Angles

Claude B. Castle and Emilio Alfaro-Bou
Langley Research Center
Hampton, Virginia

National Aeronautics
and Space Administration

**Scientific and Technical
Information Office**

1978

BLANK PAGE

SUMMARY

Three general-aviation airplane specimens, each with a mass of 2700 kg, were crash tested at 27 m/sec along flight-path angles of -15°, -30°, and -45° at the Langley impact dynamics research facility. These tests are part of a program being conducted under controlled impact conditions to determine the effects of selected impact parameters on crash response. In the present investigation, flight-path angle was the only impact parameter varied. Although other factors such as roll, yaw, pitch, velocity, angular rates, impact surface, fire, etc., can affect airplane crash behavior, such factors were not covered in this investigation.

The crash tests revealed two distinct sequential impacts: an initial impact when the fuselage nose first contacted the ground and a second impact when the cabin area in the vicinity of the wing spar contacted the ground. The second impact produced the highest accelerations in the cabin area. Changing the flight-path angle had a greater effect on structural damage and acceleration in the forward portion of the fuselage from the nose to the fire wall than in the cabin area. Structural damage to the nose section was severe at flight-path angles of -30° and -45°, but damage was moderate at a flight-path angle of -15°. At -15° and -30°, cabin volume was sufficiently maintained for the occupants to survive; at -45°, however, the "livable volume" was eliminated by the structural collapse of the cabin in the vicinity of the crew and the first passenger. The variations in normal and longitudinal acceleration magnitudes in the first-passenger pelvis from the three flight-path angles are functions of the seat structure and the crushing of the fuselage.

INTRODUCTION

With the rapid growth of private and commercial air traffic since World War II, increasing emphasis has been focused on causes of passenger injuries and deaths in severe but potentially survivable crashes. NACA (National Advisory Committee for Aeronautics), the predecessor of NASA (National Aeronautics and Space Administration), conducted a series of full-scale airplane crash tests with instrumented dummies in the early 1950's (refs. 1 and 2). These tests were performed by accelerating the airplane along a horizontal guide rail into an earthen mound. Later NACA studies shed some light on the dynamic response of seat structures to impact loads (ref. 3) and resulted in a CAA (Civil Aeronautics Administration) update in static seat strength requirements. The airplanes previously tested by NACA, however, are not structurally representative of current general-aviation airplanes. In 1973, a joint general-aviation crash-test program was initiated by the Federal Aviation Administration (FAA) and NASA.

As part of this program, NASA Langley Research Center is conducting a series of crash tests to obtain information on single- and twin-engine airplanes under controlled free-flight conditions. The variations in impact parameters

are shown in table I for the twin-engine airplanes. Objectives of the test program are to understand what happens to the structure of an airplane during a simulated crash and to learn how various impact parameters affect the magnitude and pattern of the structural damage. This information is essential for predicting structural collapse and designing new concepts for seats, occupant restraint systems, and cabin interiors. Crash-test data can also be correlated with analytical predictions using elasto-plastic, large deflection, computer programs (ref. 4).

There are certain lethal crashes in which the airplane structure is damaged beyond hope of survivability for the occupants. The crash studies at Langley Research Center, however, are directed toward those crashes in which the impacted structure retains sufficient "livable volume" for occupant survivability. A "livable volume" is a volume sufficient in size to maintain space between the occupant and the structure.

In the present investigation, three airplanes were crash tested at an impact flight-path velocity of 27 m/sec, which is approximately 70 percent of the stall for this type of airplane, along flight-path angles of -15°, -30°, and -45°. Effects of changing the flight-path angle at impact, with angle of attack and flight-path velocity being held constant, are discussed in terms of acceleration and structural damage. Other factors affecting an airplane crash such as roll, yaw, angular rates, flight-path velocities, various impact surfaces, fire, etc., are not covered here. It should be emphasized that these tests were not conducted for the purpose of evaluating the safety of a particular airplane but rather to gather data on crash phenomena which should be helpful in designing future airplanes. A motion-picture film supplement on these tests at the three flight-path angles is available on loan. A request card form and a description of the film are found at the back of this paper.

TEST FACILITY

The full-scale crash tests were performed at the Langley impact dynamics research facility shown in figure 1, and described in reference 5. The basic structure of the facility is the gantry which is 73 m high and 122 m long. A movable bridge spans the gantry at the 66-m level and can traverse the length of the gantry. A control room and an observation room are located in the building at the base of the gantry. Along the center line of the gantry at ground level is a strip of reinforced concrete 122 m long, 9.1 m wide, and 0.2 m thick which is used as the impact surface. The impact surface and a movable backboard have a painted 1-m grid system for photographic background.

The systems necessary to perform the full-scale crash tests are shown in figure 2. Swing-cable pivot-point platforms located at the west end of the gantry support the winches, sheaves, and pulley systems for controlling the length of the swing cables. A pullback platform, attached to the underside of the movable bridge, supports a winch, sheave, and pulley system for controlling the length of the pullback cable. The swing and pullback cables attached to the lifting harness which makes up the test-specimen suspension system are shown in figure 3.

The test specimen, suspended by two swing cables from the gantry, is pulled to the desired height by the pullback cable. The test sequence is initiated when the airplane is released from the pullback cable. The test specimen swings pendulum style into the impact surface as shown in figure 4. The swing cables are pyrotechnically separated prior to ground contact when the specimen is approximately 2 m from the impact surface along the flight path. The test specimen, therefore, is free from restraint during the crash sequence. The umbilical (fig. 3) remains attached during the impact for data acquisition and is pyrotechnically separated at approximately 0.75 sec after swing-cable separation.

The flight-path and attitude angles of the airplane are identified, together with the axes and force directions, in figure 5. The flight-path angle was adjusted for -15°, -30°, and -45° (see fig. 4) by varying the length of the swing cables, the longer length producing the steeper angle. The height of the test specimen was calculated to give a flight-path velocity of 27 m/sec. This velocity is the maximum obtainable at the facility for a smooth gravity induced swing and is approximately 70 percent of the stall speed for this type of airplane.

TEST SPECIMENS

Airplane specimens used for the tests were of twin-engine general-aviation type, having a nominal mass of 2700 kg and a capacity for six to eight passengers. The three airplane specimens and parameters are shown in figure 6. The -15° test specimen in figure 6(a) consists of a fuselage structural shell, wings with nacelle fairings, and landing gear. The mass and center of gravity of the empennage were simulated by two concentrated masses which represent the fin-rudder and stabilizer-elevator combinations. The ailerons and flaps were also simulated by concentrated masses. Masses were added to simulate the mass and center of gravity of the engines, propellers, and spinners; the fuel bladders were filled with colored water to simulate the fuel mass and to help locate bladder leakage, if any, during the testing; and spoilers were attached to the wings to minimize the aerodynamic lift. The -30° and -45° test specimens (figs. 6(b) and 6(c)) had all the major airplane parts and equipment of a flightworthy airplane except that the engines, propellers, and spinners were simulated as for the -15° test specimen.

The selected arrangements of seats, anthropomorphic dummies, and restraint systems are shown in figure 7. For the -30° test specimen, Hybrid II anthropomorphic dummies were used (see ref. 6), and their respective masses are given next to each dummy in figure 7. For the -15° and -45° test specimens, earlier versions of anthropomorphic dummies were used since these tests were performed chronologically earlier in the test series. The masses of these earlier dummies are also given in figure 7. The -15° and -30° test specimens did not have floor boards, instrument panel, or furnishings (except seats); whereas the -45° test specimen had floor boards, carpeting, and an instrument panel without instruments. All test specimens contained batteries, instrumentation junction boxes, pyrotechnic programer, and various electrical junction boxes and circuits needed to perform the crash test. Concentrated masses were also used

to simulate some items which are integral to a complete airplane and were arranged to provide the proper balance and center-of-gravity location of the test specimen.

INSTRUMENTATION

Onboard instrumentation consisted of accelerometers, load cells, and high-speed motion-picture cameras to provide data pertaining to the dynamic behavior of the airplane structure, cabin seats, and anthropomorphic dummies. External photographic coverage (see fig. 2) of the crash sequence was provided by tracking cameras and fixed motion-picture cameras located on each side of, in front of, and above the test specimen.

The accelerometer locations are shown in figure 8. The accelerometers were oriented in normal, longitudinal, and transverse directions. Each location - for example, 2B9N - is designated by its coordinates as follows: the first number "2" indicates the longitudinal coordinate; the first letter "B" indicates the vertical coordinate (floor to roof); the second number "9" indicates the transverse coordinate; and the second letter "N" indicates the accelerometer orientation with respect to the airplane body-axes system. (That is, the accelerometer location on the floor beam nearest the nose is designated 2B9, and the accelerometer at that location oriented in the normal direction is designated 2B9N.) The longitudinal and transverse orientations are designated L and T, respectively.

Data signals were transmitted through an umbilical cable to a junction box on top of the gantry and from there, through hard wire, to the control room where the data signals were recorded on FM tape recorders. In order to correlate data signals on the FM recorders and the external motion-picture camera data, a time code was recorded simultaneously on the magnetic tape and on the film. There was also a time-code generator onboard the airplane for use with the onboard cameras. To obtain the horizontal velocity of the airplane at impact, a Doppler radar unit was placed on the impact surface approximately 60 m aft of the impact point and the signal was recorded on one channel of the FM tapes.

The accelerometer data and data-reduction techniques are described briefly in the appendix and in reference 7. Both piezoelectric and strain-gage accelerometers were used in these tests. The output of the piezoelectric accelerometers, however, exhibited various degrees of zero shift with increasing time. This problem was compounded by the multiplicity of pulses to which each accelerometer was subjected during the tests. As a result there is some unknown error in the absolute value of accelerations recorded after the first pulse.

A casual inspection of the acceleration traces does not reveal the zero shift nor an error in the absolute value of the accelerations recorded. Only after the acceleration traces are integrated and the results are compared with known velocity values does the effect of zero shift become evident. All peak-to-peak acceleration values are believed to be accurate. Hence, data are analyzed in terms of peak-to-peak values for comparative purposes.

RESULTS AND DISCUSSION

Assessment of Structural Damage

-15° test specimen.- The photographic sequence presented in figure 9 shows the -15° test specimen at its full pullback height in the first photograph (fig. 9(a)). Figures 9(b) and 9(c) show the lifting harness controlling the glide path of the test specimen. Figure 9(d) shows the initial impact with the restraint harness separated from the test specimen so as to permit free flight at impact. The time interval of the photographic sequence, beginning with figure 9(d), is 0.05 sec. Figure 9(e) shows the crushing of the nose, and figure 9(f) shows the wings flat on the impact surface and the initial movement of the dummies. Figure 9(g) shows the slapdown of the aft fuselage section and the resulting wrinkles in the skin surface, separation of the fuselage along the lower window ledge, and the door opening. The remaining photographs (figs. 9(h) to 9(l)) show the continuing deformation of the test specimen through slide out. Inspection of these photographs indicates that the livable volume of the cabin was maintained throughout the crash sequence.

The exterior damage to the -15° test specimen is shown in figure 10. As seen in the overall view of the right side (fig. 10(a)), buckling occurred in the nose section, at the fire wall, and along the bottom of the fuselage. As shown in figures 10(c) and 10(d), there is rivet shear across the top of the fuselage aft of the pilot and copilot. Also, rivet shear is evident aft from the escape hatch along the window ledge and downward at the rear of the third window. (See figs. 10(a) and 10(b).) The breaking of the pilot's windshield and side window was due to deformation of the forward cabin section (fig. 10(a)).

Damage to the cabin interior is shown in the four photographs of figure 11. The first photograph (fig. 11(a)) is a view looking aft from the cockpit where buckling can be seen in the stiffeners which tie together the two main floor beams. Figure 11(b) is a view looking forward from the tail section and again show the main floor beams and the buckled stiffeners. The four photographs of figure 11 also show the layout of seats, dummies, additional masses, and instrumentation equipment. The apparent upward movement of the floor section is shown by the outward rotation of the seats. The view looking through the doorway, figure 11(c), and the view of the cockpit, figure 11(d), show moderate interior damage.

-30° test specimen.- The unrestrained -30° test specimen during the impact sequence is shown in figure 12. The photographic sequences are at 0.05-sec intervals, with figure 12(b) being just prior to impact. Figure 12(c) shows the crushing of the nose. The photograph of figure 12(d) shows the engine making contact and digging into the impact surface, with high longitudinal deceleration being experienced at this time. The initial movement of the dummy, as seen through the window, occurs in figure 12(d). Shown in figure 12(e) are the wing tips lying flat on the impact surface and the cabin deformation which results in the window adjacent to the first passenger being broken and the door being opened. Figure 12(h) shows the slapdown of the aft cabin section with pronounced skin buckling behind the door.

The exterior damage resulting from the crash is shown in figure 13. A view of the right side and nose section shown in figure 13(a) shows severe structural damage to the nose section, broken windshield, rivet shear, and cabin separation in the vicinity of the main spar aft of the pilot and copilot. Figures 13(b) and 13(c) are closeup views of the cabin on the right side, and figure 13(d) is a closeup view on the left side. Due to rivet shear, separation of the airframe occurred on the right side along the vertical edge of the emergency escape hatch (figs. 13(b) and 13(c)) and directly opposite on the left side (fig. 13(d)). There is rivet shear and skin separation across the top of the cabin at the rear of the escape hatch, and there is skin buckling along the roof of the cabin. Figure 13(d) shows the left side of the -30° test specimen and the cabin separation along the window ledge, the broken windows, and the collapsed nose section. The windshield center post was fractured. The deformation, tearing, and buckling of the nose of the test specimen are quite visible. Aft of the fire wall, a livable volume was maintained inside the cabin.

The interior damage to the -30° test specimen is shown in figure 14. The view looking forward from the main spar (fig. 14(a)) shows the upheaval of the floor between the pilot and copilot, with deformed cross-frame and beam-member floor supports. The crew seats remained attached to the floor although the seat support structure on the pilot seat was broken. The steel cable attached to the copilot seat did not contribute to the support of the seat but was a precautionary measure to restrain the seat and dummy had the seat detached from its floor mounts. The separation of the skin along the cross-frame member in back of the main spar is shown in figure 14(b); this view is looking forward at the right side of the test specimen, with the displaced window being the emergency escape hatch. The floor and left side of the airplane in the vicinity of the first passenger are shown in figure 14(c). The floor cross-frame supports are bent but attached, and there are buckles in the cross frame about seat-pan level along the left side. Also shown are the broken passenger window and the separation of the cabin along the window level. Figure 14(d) shows an overall view looking forward from the area behind the door. The third-passenger seat was deformed because of the apparent upward movement of the floor during the tail slapdown. (See fig. 12(h).) The cross-member supports between the two main longitudinal floor beams pulled loose from the left beam (fig. 14). In the first-passenger location, the forward movement of the dummy produced a sufficient load on the shoulder restraint system to cause tearing of the airframe structure supporting the inertial reel.

-45° test specimen.- The photographic sequence shown in figure 15 shows the -45° test specimen in free flight, impact, and slide out. The free-flight velocity of the airplane shown in figure 15(a) at 0.05 sec prior to impact is 28.6 m/sec and the pitch angle is -47.25°. The initial impact shown in figure 15(b) is followed in figure 15(c) by complete structural failure of the nose section and impact of the engines. The passenger dummies did not start responding to the impact until $t = 0.10$ sec (fig. 15(d)). Shown in figure 15(e) is the structural collapse of the cabin area which eliminates the livable volume inside the cabin in the vicinity of the crew and the first passenger. Figure 15(e) also shows the wing tip lying flat on the impact surface, which is considered a second impact for the test. The remaining frames show a quasi-reforming of the cabin volume during downward rotation of the fuselage.

In the last two frames (figs. 15(h) and 15(i)), the cabin has reformed practically to its original shape before impact, and a cursory postexamination of the crash would not have revealed the loss of livable volume which occurred inside the cabin area. This loss of livable volume established an upper boundary of -45° on flight-path angles for the overall crash-test program (table I).

The crash damage to the exterior of the -45° test specimen is shown in figure 16. An overall view of the right front side of the airplane is shown in figure 16(a) which shows the nose demolished, the windshield broken, the windshield post broken both in the center and right side, the damaged nacelle covering, and the crease across the top of the cabin section where inward folding of the roof section has taken place. Figure 16(b) is a closeup view of the right side and shows the wing-to-cabin deformation, the breakaway of the emergency escape hatch, the separation of cabin and nose section at the fire wall, and the fuel leakage. Fuel leakage occurred in both fuel tanks because of the wing structure piercing the fuel bladders. Figure 16(c) shows the cabin section from the left side and shows the fracture of the left windshield post and collapse of the first main-section frame at window level. Also shown is rivet shear along the window ledge and across the top of the cabin. Figure 16(d) is another view of the damaged cabin discussed in the previous figure (fig. 16(c)) and clearly shows the roof crease. Safety glass was used on the left windshield and plexiglass was used on the right windshield. The fragmentation pattern for both sides is shown in figure 16.

Interior cabin damage to the -45° test specimen is shown in figure 17. A view of the pilot and copilot section of the cabin (fig. 17(a)) shows the instrument panel displaced upward and the control wheel shaft broken, with the control wheel bearing on the pilot's chest. The roof impacted the head rest on the pilot seat to deform it forward, causing the dummy pilot's chin to rest on its chest. The upheaval of the cabin-floor section thrust the dummy copilot forward into the instrument panel. Figure 17(b) shows a view through the cabin door looking at the rear of the third-passenger seat. The forward motion of the third passenger during impact caused the rear seat legs of the third-passenger seat to break loose from the seat rails, as shown. The seat back is broken and the dummy's arm is visible resting in the aisle. Motion-picture coverage of the interior (see film supplement) indicates that the third seat was broken during the second impact.

The type of subfloor structural failure can be seen in the overall (fig. 17(c)) and closeup (fig. 17(d)) photographs. In figure 17(c) is shown the rivet shear along the side wall and between the cross sheet-metal frames and the longitudinal floor beams. Tearing of the sheet-metal frames is evident along the entire length of the cabin area. The closeup view (fig. 17(d)) shows the sheared rivets lying on the outer skin and the mangled cross frame structure.

Time Histories of Floor-Beam Normal Accelerations

Complete sets of the acceleration time-history traces for the airplane, for each crash test, are included in the appendix. They are presented in plots

according to their location and orientation. The locations are divided into the floor beam, cabin floor and wing, roof, and dummies.

Selected portions of accelerometer data, along the floor beam, on the floor under the first-passenger seat (fig. 7), and in the pelvis of the first passenger are presented and discussed in some detail in the following sections. Both normal and longitudinal accelerations are included.

-15° test specimen.- In figure 18(a), eight acceleration time-history traces in the normal direction from the -15° impact are presented with timed events from photographic data superimposed on the traces for correlation and interpretation. The eight accelerometers are spaced along the floor beam of the airplane from the first nose frame (2B9N) to the door of the cabin (19B9N). The response of initial ground contact is felt immediately at the first frame (2B9N) and is seen to progress rearward to the instrument panel (9B9N), with diminishing intensity and with a slight time lag associated with the rear progression of the contact surface. The nose of the airplane exhibits high amplitude oscillatory behavior caused by the repeated sequence of negative accelerations . This oscillatory behavior is due to load transmission through structural failures and load build-up, thereby relieving load momentarily on undamaged structure and causing subsequent structural deceleration loading. This cycle is repeated as various structural elements are loaded and successively fail. Main spar ground contact (0.048 sec) produces a downward force in the nose of the airplane (positive acceleration) and signals the initiation of cabin compartment excitation. Acceleration peaks in the cabin compartment are a maximum in the vicinity of the main spar and diminish progressively from that point rearward. At 0.091 sec (fig. 18(a)) the loss of wing dihedral angle and wing ground contact occurs, thus resulting in the twisting of the main spar. At this time, peak-to-peak accelerations of 130g and 50g are produced in the first-passenger aisle seat legs (15B9N and 17B9N).

-30° test specimen.- Seven normal accelerations along the floor beam for the -30° impact are shown in figure 18(b). Accelerometer locations are similar to those of the -15° impact (fig. 8), except for the removal of the accelerometer from the middle of the luggage compartment in the nose of the airplane (4B9N at -15° impact). The response at initial ground contact in the nose of the airplane is severe and is seen to progress rearward to the instrument panel (9B9N) with diminishing intensity. The maximum peak-to-peak acceleration at the fire wall (9B9N) is 190 percent higher for the -30° impact than for the -15° impact.

Severe local accelerations in the vicinity of the floor under the instrument panel (9B9N) indicate structural vibrations (0.065 sec). The ground contact is seen to progress from the nose of the airplane rearward through the cabin area. The intensity of the accelerations in the cabin area increases markedly as the cabin first begins to make contact with the ground (0.085 sec) and the door begins to open. The main spar contact occurs at 0.107 sec and coincides with a large peak-to-peak acceleration of approximately 70g (15B9N) and 46g (16B9N) in the first-passenger seat; also, it causes loss of an accelerometer (18B9N) in the front aisle leg of the third-passenger seat. A second acceleration pulse occurs in the rear of the third-passenger seat (19B9N) when

the floor starts to buckle upward (0.230 sec at 40g) and the rear of the cabin makes ground contact in the vicinity of the door.

-45° test specimen.- Seven normal accelerations along the floor beam for the -45° impact are shown in figure 18(c). The accelerometer locations are similar to those of -30° impact (fig. 8). The response at initial ground contact in the nose of the airplane is most severe for the -45° impact; in fact, peak-to-peak accelerations as high as 310g are induced. On moving rearward after the progression of the impact pulse, the magnitudes of the acceleration decrease as some of the impact energy is absorbed by the nose structure and less difference in magnitude is evident between the -15°, -30°, and -45° acceleration traces in the cabin area of the three test specimens. Overall, the duration of accelerations is shorter and less severe in the -15° impact than in the -30° impact or in the -45° impact. (See figs. 18(a), 18(b), and 18(c).)

Time Histories of Floor-Beam Longitudinal Accelerations

In figure 19, time histories of fuselage floor-beam longitudinal accelerations are presented for the -15°, -30°, and -45° test specimens, with timed events from photographic data superimposed on the traces for correlation and interpretation.

-15° test specimen.- Seven accelerometers (fig. 19(a)) are spaced along the floor beam of the airplane from the first nose frame (2B9L) to the rear of the passenger seat (19B9L). The response at initial ground contact is felt immediately at the first frame (2B9L), and contact progresses rearward to the instrument panel (9B9L) with diminishing intensity but with about half the acceleration magnitudes experienced in the normal direction. Similarly, a characteristic high-amplitude oscillatory behavior in the nose of the airplane in the vicinity of the main spar is again evident for the longitudinal accelerations as for the normal accelerations. Wing ground contact (second impact) is shown at 0.091 sec. The time at which fuselage separation occurred (across the cabin roof in the vicinity of the main spar) coincides with the positive acceleration peak in 17B9L and 19B9L at 0.164 sec.

-30° test specimen.- There are seven longitudinal accelerometer locations along the floor beam in the -30° impact test. The additional accelerometer location 18B9L was added when a passenger and seat were placed in the third-passenger position (fig. 7). The longitudinal accelerations for the -30° test specimen are shown in figure 19(b). The accelerometer below the instrument panel (9B9L) shows a peak-to-peak acceleration 340 percent greater for the -30° test specimen than for the -15° test specimen. The longitudinal peak-to-peak accelerations in the cabin area (15B9L to 19B9L) show an increase of approximately 130 percent over the -15° cabin accelerations. The change in flight-path angle has much greater effect on the nose to fire wall portion of the airplane than in the passenger compartment. The third-passenger seat begins to deform, as determined from motion-picture data at wing ground contact.

-45° test specimen.- In figure 19(c), eight longitudinal acceleration traces along the floor beam for the -45° test specimen are presented. The additional accelerometer location 20B9L was added when a passenger and seat

were placed in the third-passenger position (fig. 7). The magnitude of the longitudinal acceleration from the nose to the fire wall is about the same for the -45° test specimen as for the -30° test specimen. The longitudinal accelerations in the cabin area are also comparable to those of the -30° test specimen, thus indicating that severe structural deformations, which limit the magnitudes of the accelerations, are taking place. Also evident are inconsistencies in individual acceleration traces at approximately the same fuselage location - 9B9L and 18B9L at -30° and 9B9L and 17B9L at -45° - with much higher accelerations at -30°. These inconsistencies can be attributed to severe local structural failures changing the character of the local response. Wing ground contact at 0.120 sec to maximum closure of the cabin interior at 0.171 sec corresponds to the maximum longitudinal accelerations in the cabin interior with the maximum longitudinal acceleration occurring near maximum cabin closure (0.158 sec). After maximum cabin closure, the cabin began to reform as the airplane tail rotated to a horizontal position and continued its horizontal slide-out for approximately 30 m.

Profiles of Floor-Beam Maximum Peak-to-Peak Normal and Longitudinal Accelerations

Figure 20 shows a profile of the normal and longitudinal peak-to-peak accelerations along the floor beam for the -15°, -30°, and -45° test specimens. From the profile, the highest and lowest peak-to-peak levels and their locations along the floor beam can be determined.

The average of the highest peak-to-peak accelerations along the floor beam in the normal direction for the -30° and -45° test specimens was less than twice that of the -15° test specimen; whereas in the longitudinal direction, the average for the -30° and -45° test specimens was three to four times that of the -15° test specimen.

At all three flight-path angles, the higher longitudinal acceleration levels were experienced forward of the main spar and the lower levels were experienced toward the rear of the cabin. At -45°, the nose end of the airplane was completely crushed, energy was absorbed, and load paths were redistributed - accounting for some load alleviation and lower peak-to-peak acceleration levels on the floor beam than at -30°. The normal and longitudinal maximum peak-to-peak levels were of approximately the same value for the -45° tests.

For the -15° test specimen, the normal peak-to-peak acceleration levels (fig. 20(a)) were more than twice the longitudinal acceleration levels (fig. 20(b)). This was due to higher decelerations in the normal direction when the airplane contacted the impact surface and abruptly stopped the motion in that direction. However, after initial impact in the longitudinal direction, the airplane skidded for some distance and then came to a stop; this long skid distance contributed to lower longitudinal deceleration forces. In figure 20(b) the longitudinal levels are shown to be nearly constant for the entire length of the floor beam, thus indicating little floor-beam deformation for the -15° test specimen but severe structural collapse and floor-beam deformations for the -30° and -45° test specimens. The effect of changes in flight-path angle

is more evident in the forward portion of the fuselage (forward of the main spar) than in the cabin area for the three nose-down impact tests.

Accelerations on Cabin Seats and Occupants

The normal accelerations on the floor under the seat and on the pelvis of the first passenger are presented in figure 21. Accelerometers were mounted adjacent to each of the four seat legs.

The longitudinal accelerations in the floor beam adjacent to the legs of the first-passenger seat are shown in figure 22. The front seat leg locations experienced higher longitudinal deceleration loads than did the rear seat leg locations as the occupant moved forward upon impact.

Normal accelerations at -15°.- Figure 21(a) shows the normal accelerations for the -15° test specimen. Peak-to-peak accelerations of 130g and 81g were recorded on the floor under the two front seat legs at the first-passenger location, and accelerations of 76g (58 percent of 130g) were recorded in the pelvis approximately 0.025 sec later. The peak-to-peak accelerations under the rear seat legs were 60g and 80g and corresponded to a 36g pulse (45 percent of 80g) on the pelvis - again with a delay of approximately 0.025 sec.

Normal accelerations at -30°.- Figure 21(b) shows the normal accelerations for the -30° test specimen. Peak-to-peak accelerations of 70g and 68g were recorded on the floor under the two front seat legs and 45g and 32g under the two rear seat legs. The acceleration on the pelvis was recorded at 40g (15 percent of 70g) approximately 0.02 sec later.

The -30° test specimen was the only one in which the restraint system of the first passenger was instrumented with load cells. The positive (downward) peak-to-peak accelerations of 60g (fig. 21(b)) in the pelvis corresponded to a 5.3-kN tensile force in the shoulder harness (see appendix fig. A3(f)) when the occupant's relative motion with respect to the seat was stopped by the restraint system.

Normal accelerations at -45°.- Some unusual airplane crash behavior was exhibited by the -45° test specimen during impact. First, the nose of the airplane impacted and crushed progressively to the fire wall while the remaining portion of the fuselage maintained its -45° flight-path angle, thus eliminating the livable volume in the cabin. This behavior was followed by a downward rotation and a reforming of the fuselage immediately thereafter. The resulting accelerations (fig. 21(c)) on the floor and in the pelvis of the first passenger lacked the smoothness and well-defined pelvic pulse of the -15° and -30° test specimens. Nevertheless, peak-to-peak accelerations on the floor were 80g and 65g next to the front seat legs and 60g and 80g next to the rear seat legs. The peak-to-peak acceleration on the pelvis was 30g (38 percent of 80g), which occurred at about 0.015 sec later. The seat deformed, absorbing some of the impact energy and reducing the pelvic accelerations.

Effects of normal accelerations.- The pelvis peak-to-peak accelerations in the -15°, -30°, and -45° test specimens were 76g (fig. 21(a)), 40g (fig. 21(b)),

and 30g (fig. 21(c)), respectively. The 76g acceleration reflects the effect of cabin slapdown on the impact surface. A positive 60g peak-to-peak pulse was due to the effect produced by the dummy lifting off the seat against the restraint system. The 30g acceleration reflects the effect energy absorption plays in reducing load transmission. A greater total seat deformation was obtained in the -45° test specimen than was obtained in either the -15° or -30° test specimens. This situation suggests that accelerations experienced in aircraft crashes are limited by the eventual collapse of the surrounding structure. Unfortunately, this structural collapse may also be accompanied by the loss of a livable volume within the cabin area, affecting the survivability of the occupant. In a crashworthy design, the structural collapse would be controlled to produce maximum energy absorption and still maintain livable volume in the cabin.

Longitudinal accelerations at -15°.- As shown for the -15° test specimen in figure 22(a), longitudinal peak-to-peak accelerations of 40g and 50g were recorded adjacent to the front seat legs and 35g and 12g adjacent to the rear seat legs. These acceleration pulses were recorded in the pelvis with a peak-to-peak value of 115g occurring 0.025 sec later.

Longitudinal accelerations at -30°.- As shown for the -30° test specimen in figure 22(b), longitudinal peak-to-peak accelerations of 120g and 40g were recorded on the floor adjacent to the front seat legs and 65g and 40g adjacent to the rear seat legs. These peaks were recorded in the pelvis as a 40g peak-to-peak pulse occurring 0.025 sec later.

Longitudinal accelerations at -45°.- As shown for the -45° test specimen in figure 22(c), longitudinal peak-to-peak accelerations adjacent to each of the four seat legs were approximately the same: 40g for the two front legs and 35g for the two rear seat legs. The pelvis also experienced the same value as the two rear legs of 35g occurring 0.025 sec later.

Effects of normal and longitudinal accelerations.- The -15° longitudinal accelerations have a higher peak-to-peak pelvic magnitude (115g) than the equivalent normal pelvic deceleration pulse (76g). The -30° normal and longitudinal peak-to-peak pelvic accelerations are the same (40g), and the -45° normal and longitudinal pelvic accelerations are also of the same order of magnitude (30g and 35g). The type of restraint system could have an influence on the loadings experienced by the occupant.

SUMMARY OF RESULTS

Three full-scale twin-engine airplane specimens were crash tested at flight-path angles of -15°, -30°, and -45° with a constant flight-path velocity of 27 m/sec. These tests were part of a program to investigate airplane response to controlled crash conditions. The results are summarized in the following observations:

1. Structural damage to the nose section was severe in the -30° and -45° test specimens but only moderate in the -15° test specimen. In the -15° test specimen, the floor beams and supporting frames exhibited moderate buckling,

but both buckling and rivet shear of the subfloor structure occurred in the -30° test specimen and the -45° test specimen.

2. A livable cabin volume was maintained in the -15° and -30° test specimens, but for the -45° test specimen the structural collapse of the cabin eliminated the livable volume inside the cabin in the vicinity of the crew and first passenger. This loss of livable cabin volume established an upper boundary of -45° on flight-path angles.

3. The effects of change in flight-path angle are evident in the peak-to-peak accelerations in the forward portion of the fuselage, from the nose to the fire wall, but are not as evident in the cabin area.

4. All three test specimens exhibited rivet shear across the top of the fuselage in the vicinity of the main spar and along the window ledge. The peak-to-peak accelerations in the cabin area are higher forward of the main spar and diminish progressively from that point rearward. These test results suggest that the peak-to-peak accelerations during the crash sequence are limited by the eventual collapse of the surrounding airplane structure.

5. The first-passenger pelvis peak-to-peak normal accelerations in the -15°, -30°, and -45° test specimens were 76g, 40g, and 30g, respectively, and the longitudinal peak-to-peak accelerations were 115g, 40g, and 35g. These variations in accelerations are attributed to the flight-path angle, to the restraint system, and to the collapse of the seat structure.

6. The average of the highest peak-to-peak accelerations along the floor beam in the normal direction for the -30° and -45° test specimens was less than twice that of the -15° test specimen; whereas in the longitudinal direction the average for the -30° and -45° test specimens was three to four times that of the -15° test specimen.

Langley Research Center
National Aeronautics and Space Administration
Hampton, VA 23665
May 2, 1978

REFERENCES

1. Preston, G. Merritt; and Moser, Jacob C.: Crash Loads. NACA Conference on Airplane Crash-Impact Loads, Crash Injuries and Principles of Seat Design for Crash Worthiness (Cleveland, Ohio), Apr. 1956, pp. 2-1 - 2-47.

2. Eiband, A. Martin; Simpkinson, Scott H.; and Black, Dugald O.: Accelerations and Passenger Harness Loads Measured in Full-Scale Light-Airplane Crashes. NACA TN 2991, 1953.

3. Pinkel, I. Irving; and Rosenberg, Edmund G.: Seat Design for Crash Worthiness. NACA Rep. 1332, 1957. (Supersedes NACA TN 3777.)

4. Alfaro-Bou, E.; Hayduk, R. J.; Thomson, R. G.; and Vaughan, V. L., Jr.: Simulation of Aircraft Crash and Its Validation. Aircraft Crashworthiness, Kenneth Saczalski, George T. Singley III, Walter D. Pilkey, and Ronald L. Huston, eds., Univ. Press of Virginia, c.1975, pp. 485-497.

5. Vaughan, Victor L., Jr.; and Alfaro-Bou, Emilio: Impact Dynamics Research Facility for Full-Scale Aircraft Crash Testing. NASA TN D-8179, 1976.

6. Humanoid Systems. Report on Part 572 (GM HYBRID-II) Anthropomorphic Test Dummy. Alderson Biotechnology Corp., Jan. 31, 1974.

7. Alfaro-Bou, Emilio; and Vaughan, Victor L., Jr.: Light Airplane Crash Tests at Impact Velocities of 13 and 27 m/sec. NASA TP-1042, 1977.

TABLE I.- IMPACT PARAMETERS FOR TWIN-ENGINE AIRPLANE SPECIMENS

Flight path, deg	Pitch angle, deg	Roll angle, deg	Yaw angle, deg	Angle of attack, deg	Velocity, m/sec	Source
-15	-15	0	0	0	13	Reference 7
[a]-15	-15	0	0	0	[b]27	Reference 7 and present paper
[a]-30	-30	0	0	0	27	Present paper
[a]-45	-45	0	0	0	27	Present paper
-15	0	0	0	15	27	
-15	15	0	0	30	27	
-15	-15	-15	0	0	27	
-15	-15	-30	0	0	27	

[a]Specifically discussed in present paper.
[b]Maximum velocity for free fall due to height limitation.

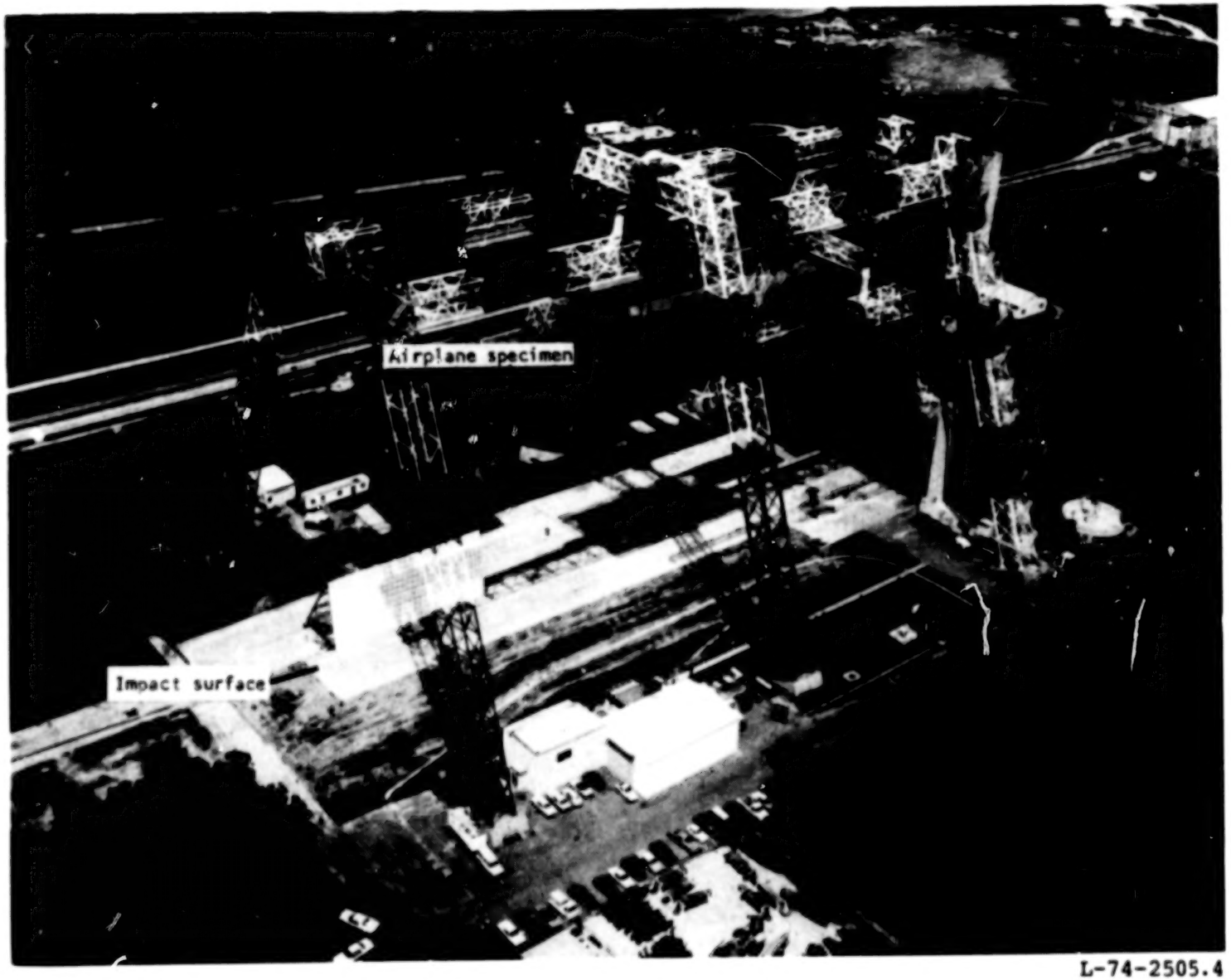

L-74-2505.4

Figure 1.- Langley impact dynamics research facility.

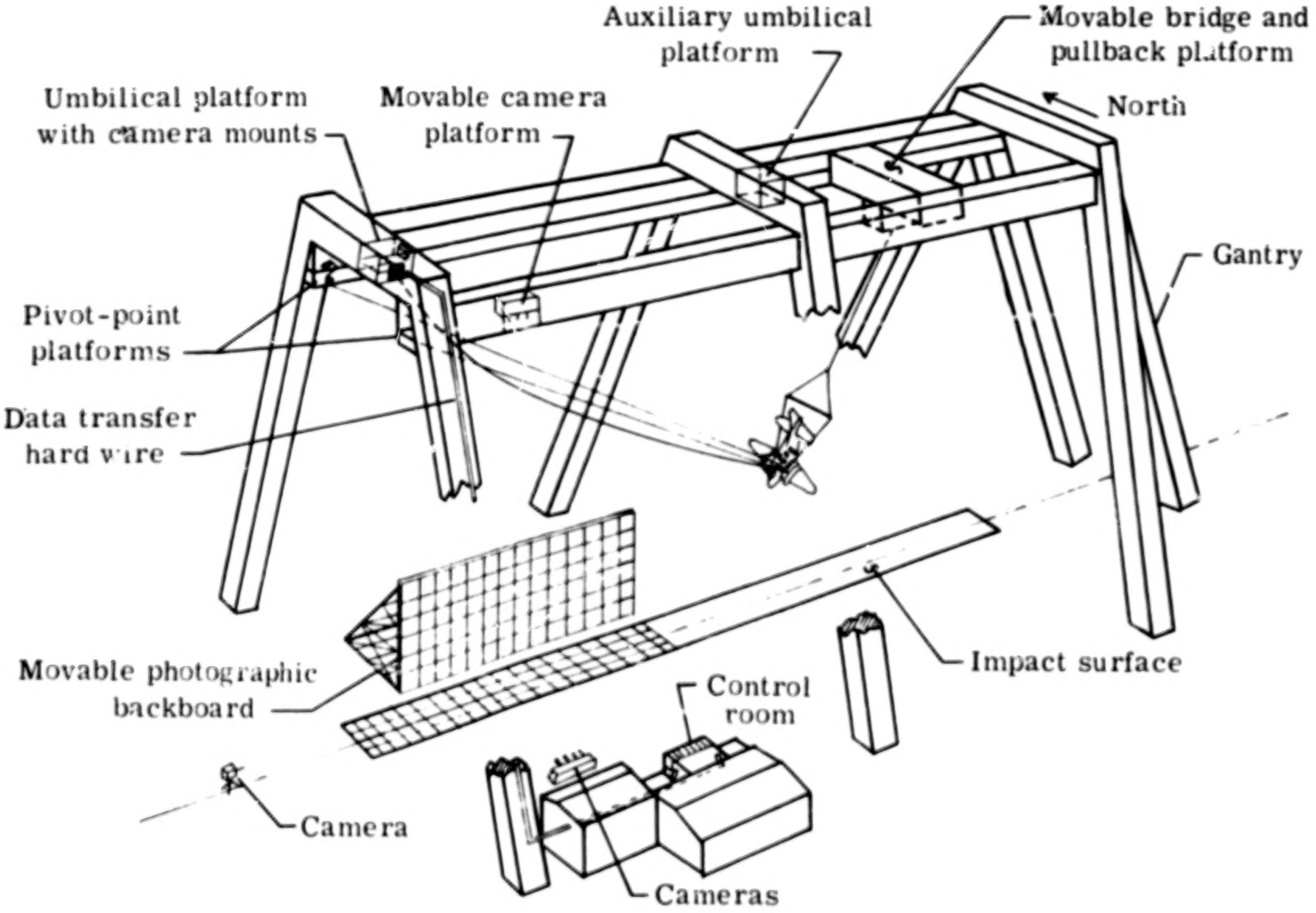

Figure 2.- Diagram of Langley impact dynamics research facility.

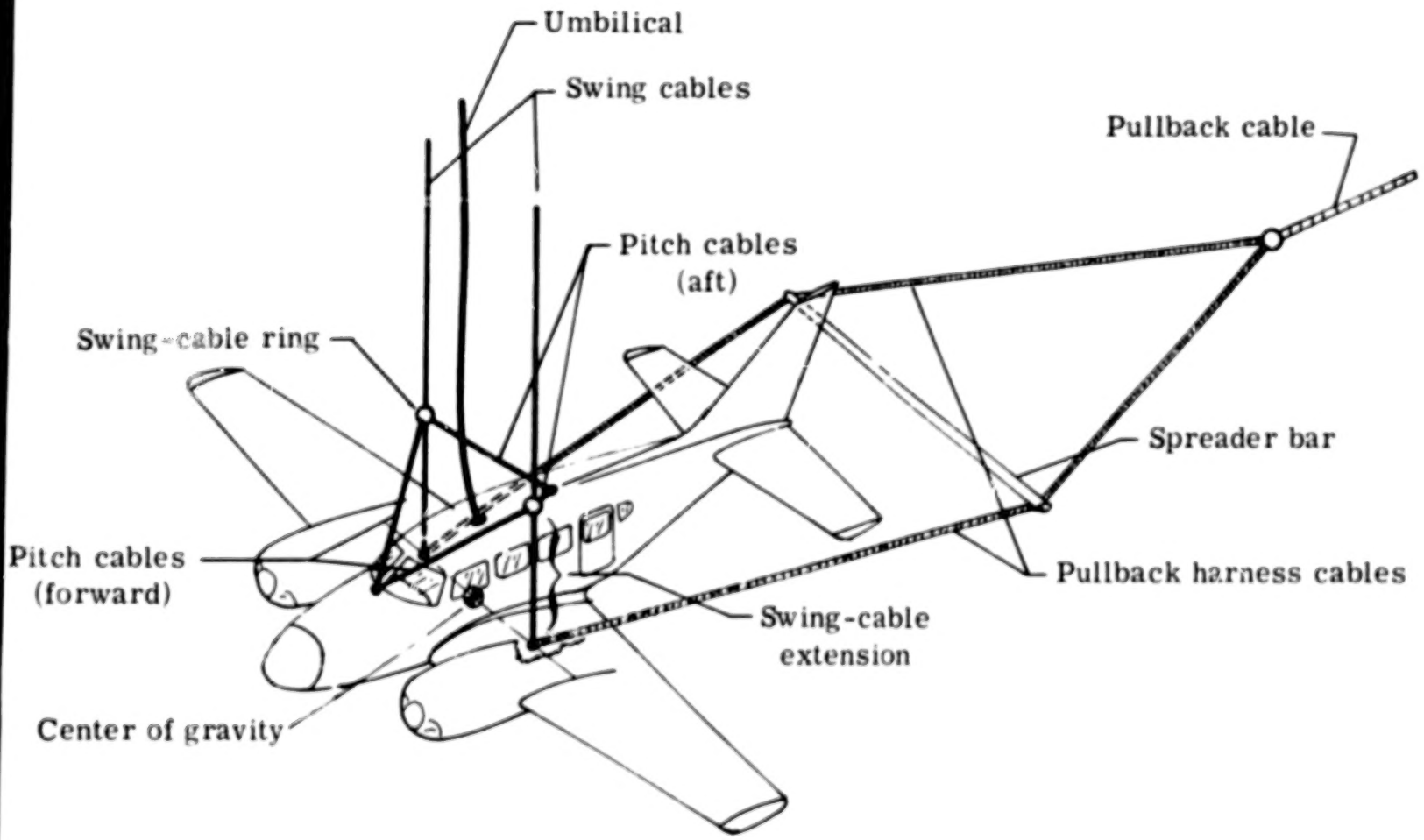

Figure 3.- Test-specimen suspension system.

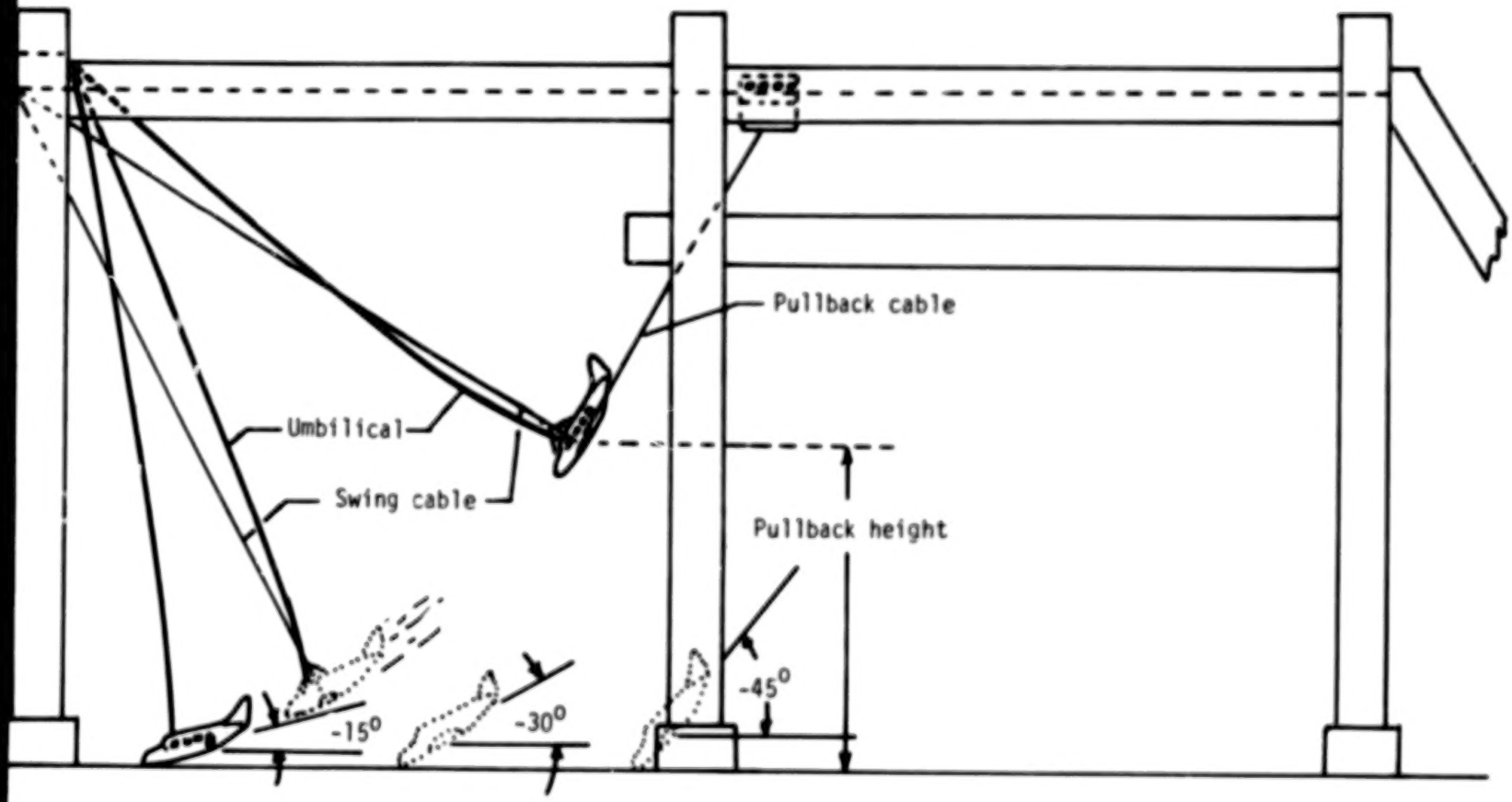

Figure 4.- Crash sequence of test specimen.

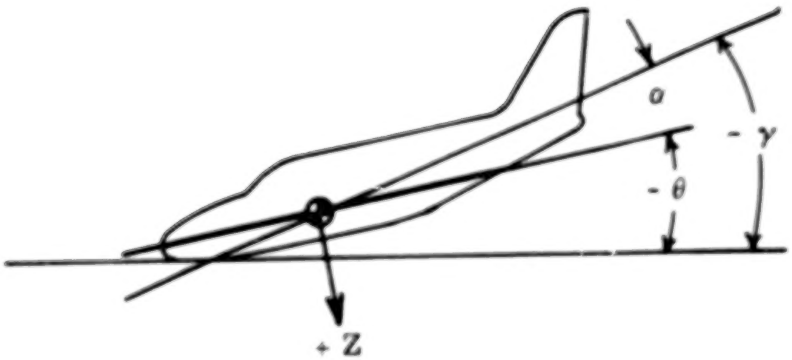

γ Flight-path angle

α Angle of attack

θ Pitch angle,

$\theta = \gamma + \alpha$

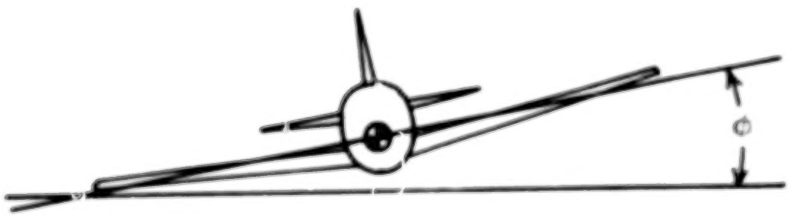

ϕ Roll angle

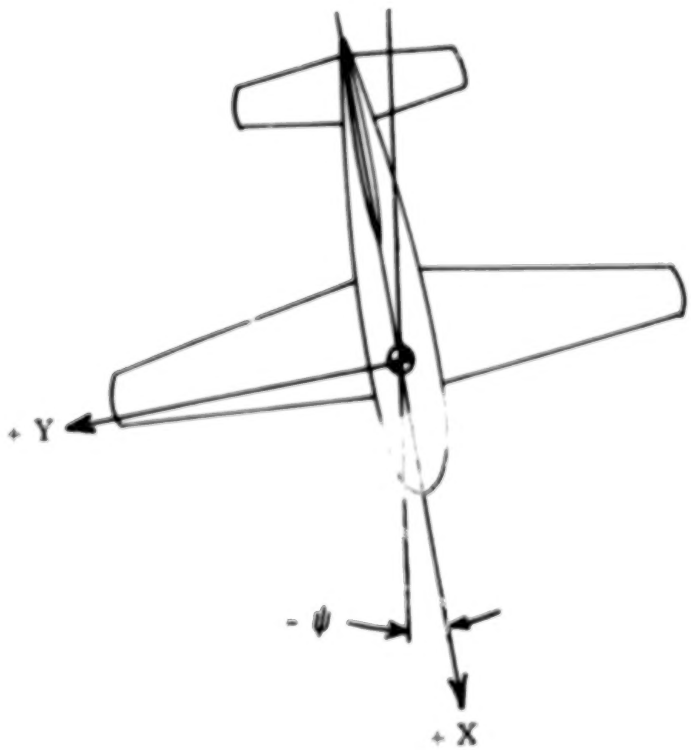

ψ Yaw angle

Figure 5.- Coordinate system and crash attitude.

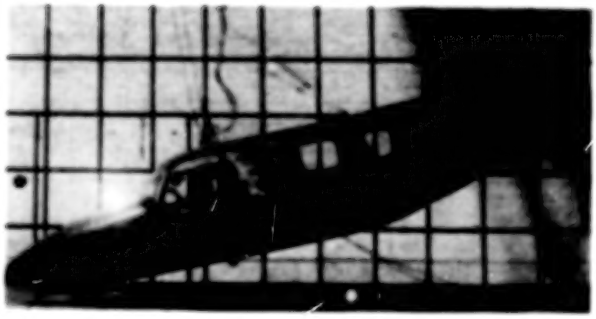

Test parameter	Planned	Actual
Flight path, deg	-15.0	-16.0
Free-flight time, sec	0.07	0.07
Angle of attack, deg	0.0	4.0
Pitch angle, deg	-15.0	-12.0
Yaw angle, deg	0.0	1.5
Roll angle, deg	0.0	0.0
Flight-path velocity, m/sec	26.8	26.6
Vertical velocity, m/sec	6.9	7.3
Horizontal velocity, m/sec	25.9	25.6

(a) -15° test specimen.

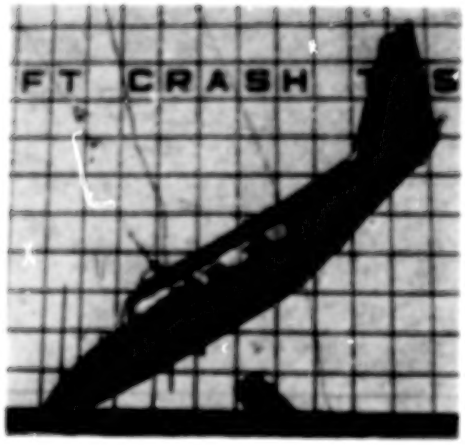

Test parameter	Planned	Actual
Flight path, deg	-30.0	-30.0
Free-flight time, sec	0.07	0.06
Angle of attack, deg	0.0	1.2
Pitch angle, deg	-30.0	-31.2
Yaw angle, deg	0.0	2.0
Roll angle, deg	0.0	-1.0
Flight-path velocity, m/sec	26.8	27.6
Vertical velocity, m/sec	13.4	13.8
Horizontal velocity, m/sec	23.2	23.9

(b) -30° test specimen.

Test parameter	Planned	Actual
Flight path, deg	-45.0	-47.5
Free-flight time, sec	0.07	0.03
Angle of attack, deg	0.0	0.2
Pitch angle, deg	-45.0	-47.2
Yaw angle, deg	0.0	2.5
Roll angle, deg	0.0	0.0
Flight-path velocity, m/sec	26.8	28.6
Vertical velocity, m/sec	19.0	21.1
Horizontal velocity, m/sec	19.0	19.3

(c) -45° test specimen.

Figure 6.- Test specimens and test parameters. L-78-94

(a) -15° test specimen.

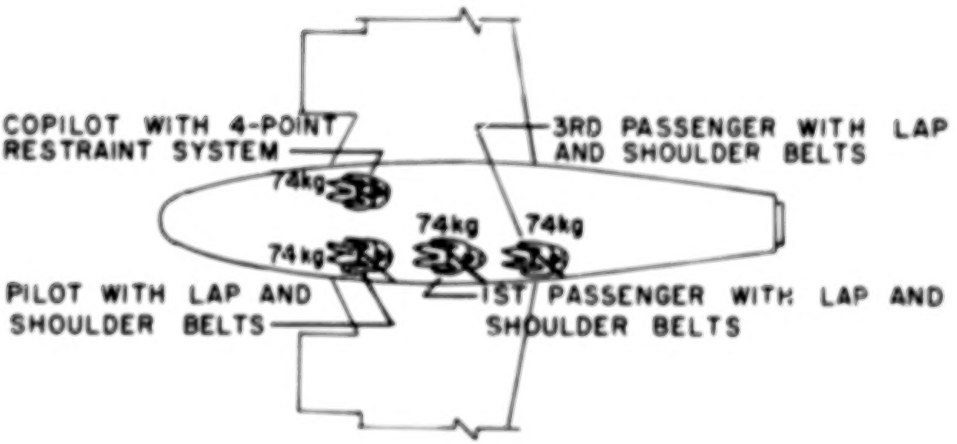

(b) -30° test specimen.

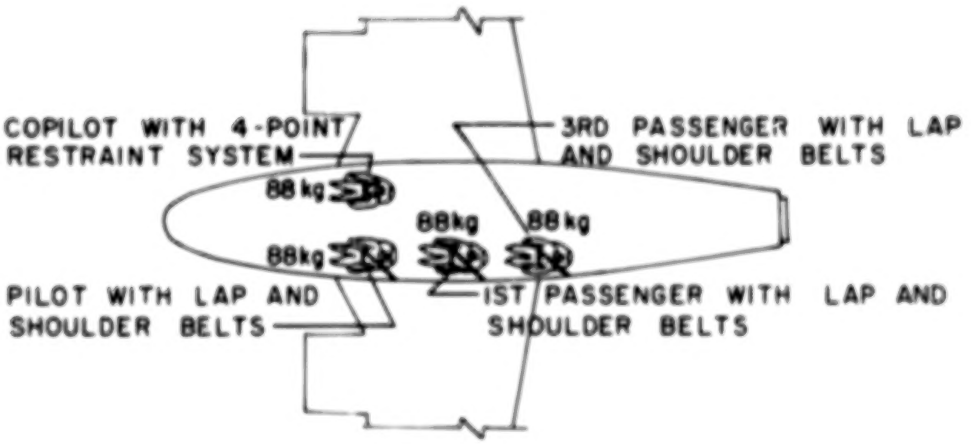

(c) -45° test specimen.

Figure 7.- Arrangement of seats, dummies, and restraint systems for various flight-path test specimens.

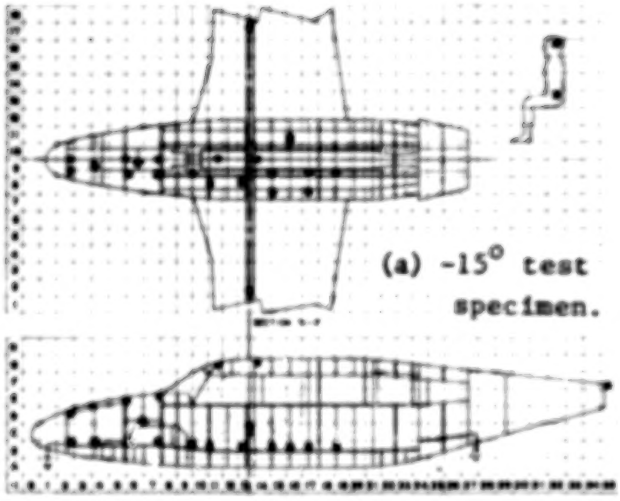

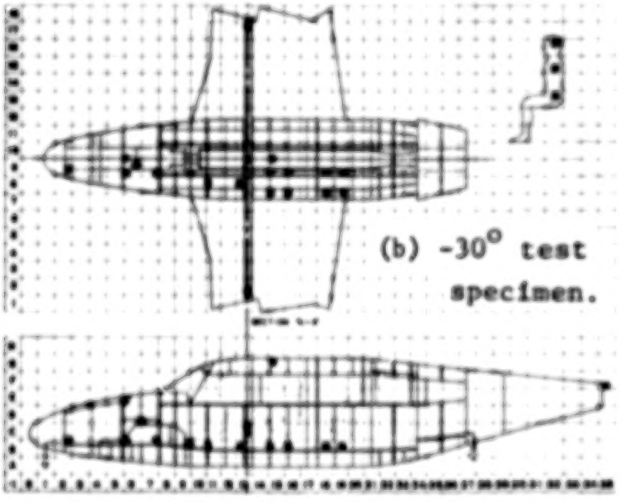

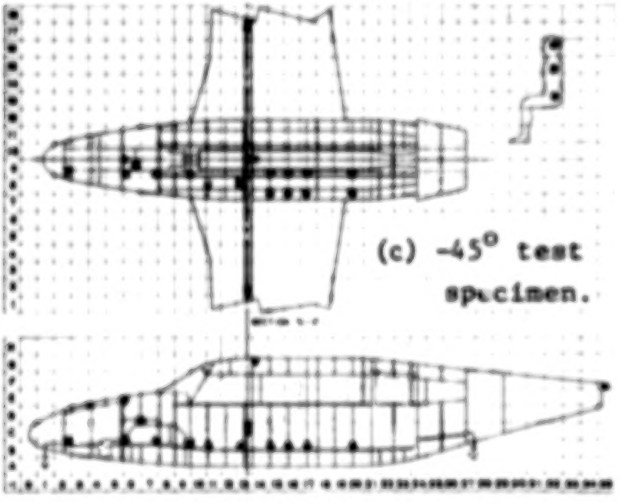

Accelerometer identification

- Floor
- Roof and tail
- Wheel well and wings
- Pilot and 1st passenger

Accelerometers in dummies	
Pilot, pelvic, normal	11C5
Pilot, pelvic, longitudinal	11C6
Pilot, head, normal	12F6
Pilot, head, longitudinal	12F5
1st passenger, pelvic, normal	16C6
1st passenger, pelvic, longitudinal	16C5
1st passenger, head, normal	16F6
1st passenger, head, longitudinal	16F5

Accelerometers in dummies	
Copilot, pelvic, normal	11C11
Pilot, pelvic, normal	11C6
Pilot, pelvic, longitudinal	11C5
Pilot, chest, normal	12E6
Pilot, chest, longitudinal	12E5
Pilot, head, normal	12F6
Pilot, head, longitudinal	12F5
1st passenger, seat pan, normal	16C8
1st passenger, pelvic, normal	16C6
1st passenger, pelvic, longitudinal	16C5
1st passenger, chest, normal	16E6
1st passenger, chest, longitudinal	16E5
1st passenger, head, normal	16F6
1st passenger, head, longitudinal	16F5
3rd passenger, seat pan, normal	19C8
3rd passenger, pelvic, normal	19C6
3rd passenger, pelvic, longitudinal	19C5
3rd passenger, chest, normal	20E6
3rd passenger, chest, longitudinal	20E5
3rd passenger, head, normal	20F6
3rd passenger, head, longitudinal	20F5
Load cells—restraint belts	
Pilot, shoulder	11D8
1st passenger, lap	15D8
1st passenger, shoulder	15D6
3rd passenger, lap	19D8
3rd passenger, shoulder	19D6

Accelerometers in dummies	
Copilot, pelvic, normal	11C11
Pilot, pelvic, normal	11C6
Pilot, pelvic, longitudinal	11C5
Pilot, chest, normal	12E6
Pilot, chest, longitudinal	12E5
Pilot, head, normal	12F6
Pilot, head, longitudinal	12F5
1st passenger, seat pan, normal	16C8
1st passenger, pelvic, normal	16C6
1st passenger, pelvic, longitudinal	16C5
1st passenger, chest, normal	16E6
1st passenger, chest, longitudinal	16E5
1st passenger, head, normal	16F6
1st passenger, head, longitudinal	16F5
3rd passenger, seat pan, normal	19C8
3rd passenger, pelvic, normal	19C6
3rd passenger, pelvic, longitudinal	19C5
3rd passenger, chest, normal	20E6
3rd passenger, chest, longitudinal	20E5
3rd passenger, head, normal	20F6
3rd passenger, head, longitudinal	20F5

Figure 8.- Accelerometer locations on test specimens and in dummies.

(a) Pullback position.

(b) Before impact.

(c) Before impact.

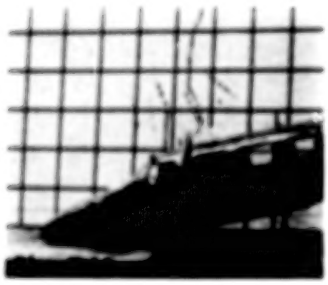

(d) Initial impact; Time = 0 sec.

(e) Time = 0.05 sec.

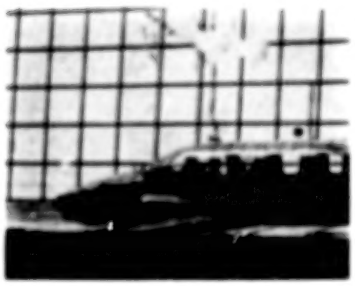

(f) Time = 0.10 sec.

(g) Time = 0.15 sec.

(h) Time = 0.20 sec.

(i) Time = 0.25 sec.

(j) Time = 0.30 sec.

(k) Time = 0.35 sec.

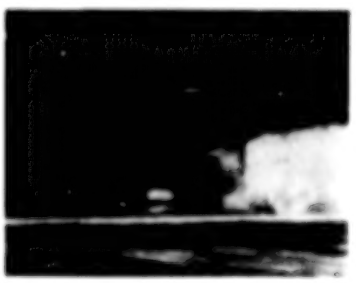

(l) Time = 0.40 sec.

L-74-2693

Figure 9.- Photographic sequence of -15° test specimen.

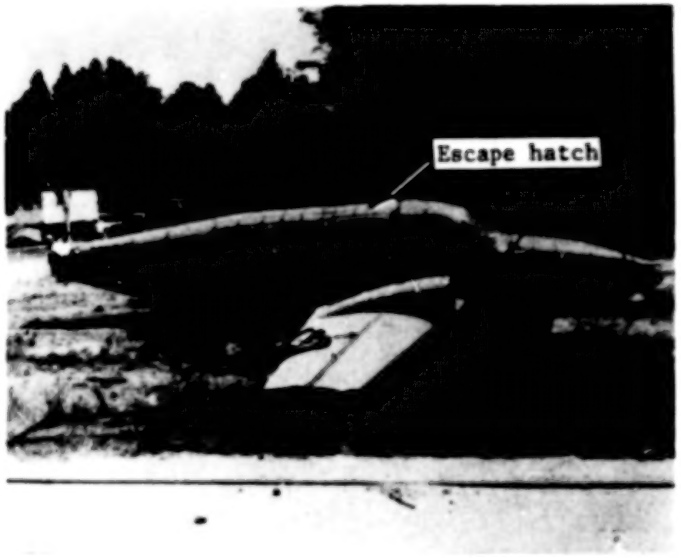

(a) Overall view of right side.

(b) Closeup view of right side.

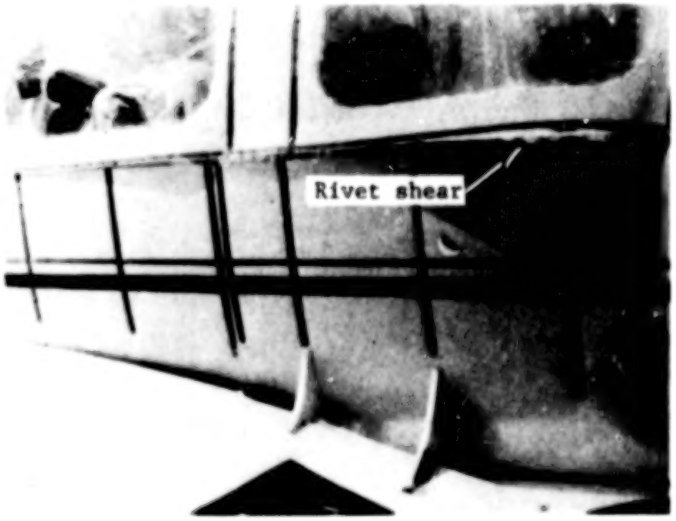

(c) Closeup view of left side.

(d) Closeup view of left side and top of fuselage.

L-78-95

Figure 10.- Exterior damage to -15° test specimen.

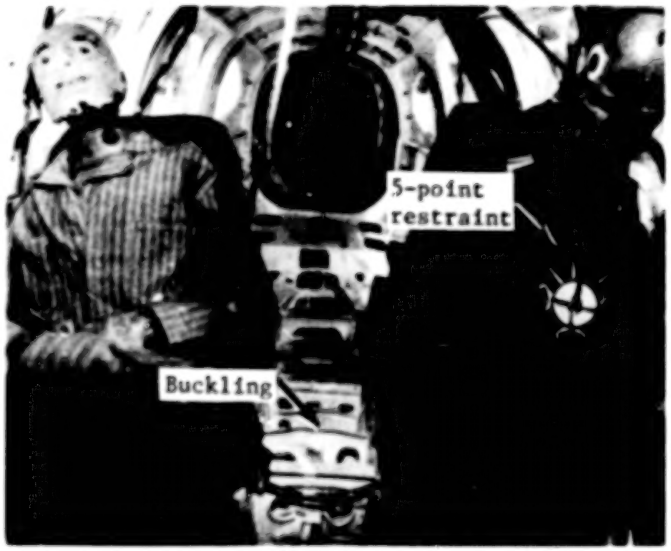

(a) View looking rearward.

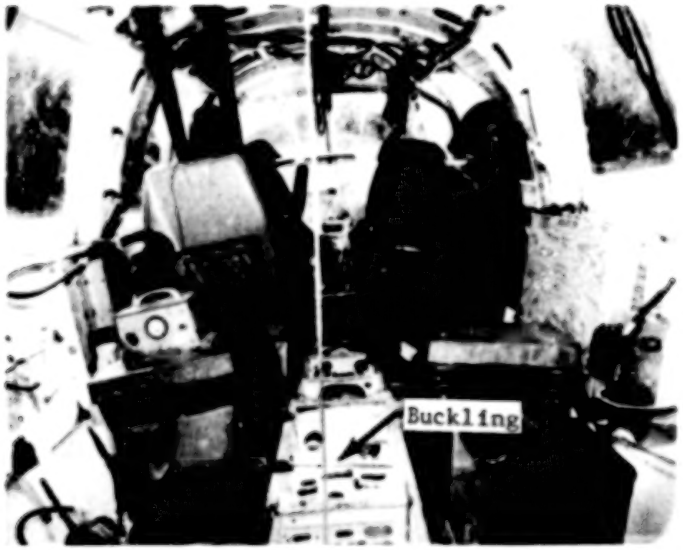

(b) View looking forward.

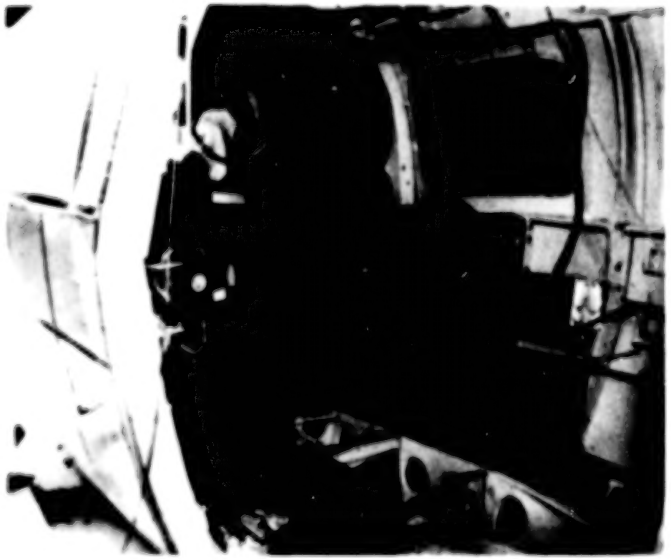

(c) View through doorway.

(d) View of cockpit area.

L-78-96

Figure 11.- Interior damage to -15° test specimen.

(a) Prior to impact.

(b) Time = -0.01 sec.

(c) Time = 0.04 sec.

(d) Time = 0.09 sec.

(e) Time = 0.14 sec.

(f) Time = 0.19 sec.

(g) Time = 0.24 sec.

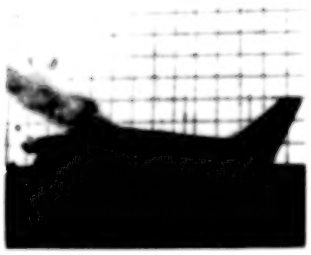

(h) Time = 0.29 sec.

(i) Time = 0.34 sec.

(j) Time = 0.39 sec.

(k) Time = 0.44 sec.

(l) Time = 0.49 sec.

L-78-97

Figure 12.- Photographic sequence of -30° test specimen.

(a) View of right side and nose.

(b) Closeup view of cabin.

(c) View of right side.

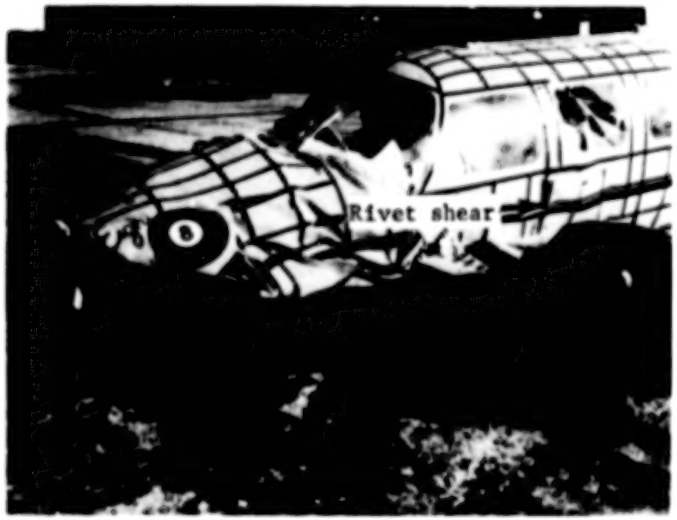

(d) View of left side, nose, and cabin.

L-78-98

Figure 13.- Exterior damage to -30° test specimen.

(a) View of cockpit area.

(b) View of right side at main spar.

(c) View of floor and left side.

(d) View looking forward in cabin area.

L-78-99

Figure 14.- Interior damage to -30° test specimen.

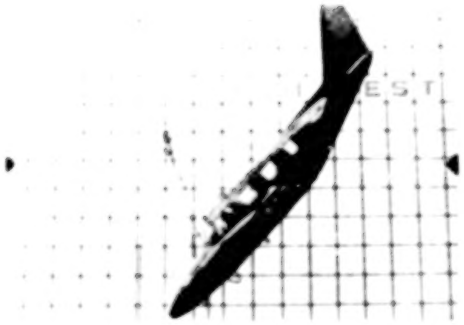

(a) Prior to impact.

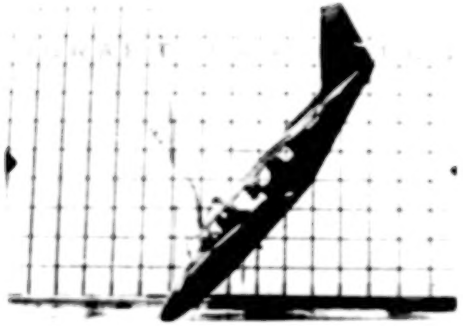

(b) Initial impact; Time = 0 sec.

(c) Time = 0.05 sec.

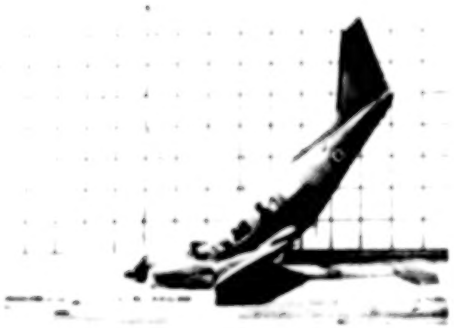

(d) Time = 0.10 sec.

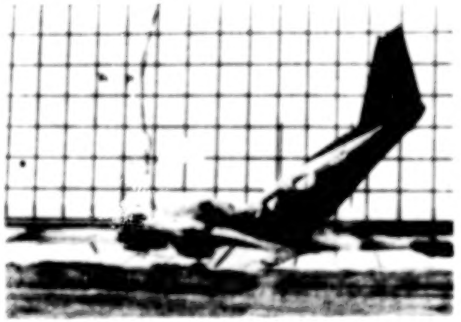

(e) Time = 0.15 sec.

(f) Time = 0.20 sec.

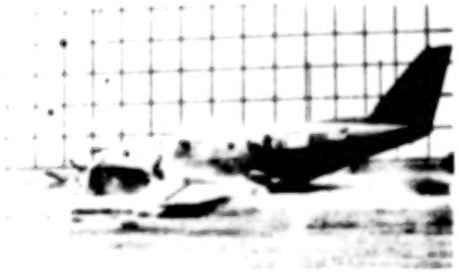

(g) Time = 0.25 sec.

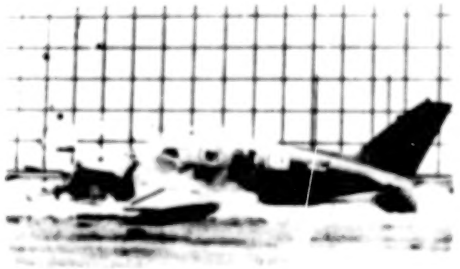

(h) Time = 0.30 sec.

(i) Time = 0.35 sec.

L-78-100

Figure 15.- Photographic sequence of -45° test specimen.

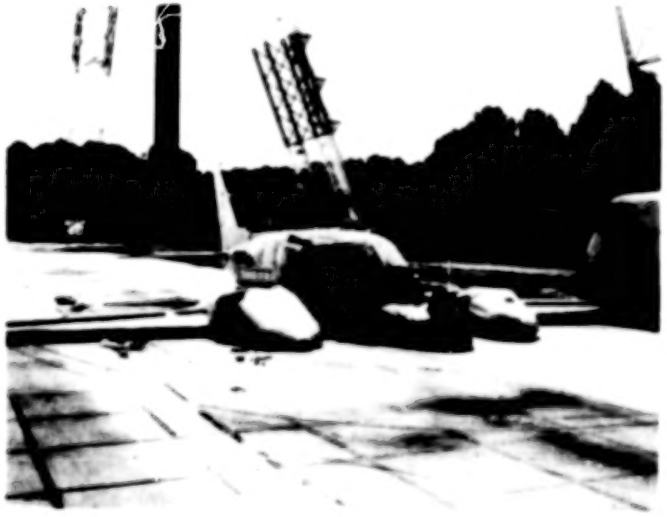

(a) Overall view of right front side.

(b) Closeup view of right side.

(c) View of left side of cabin.

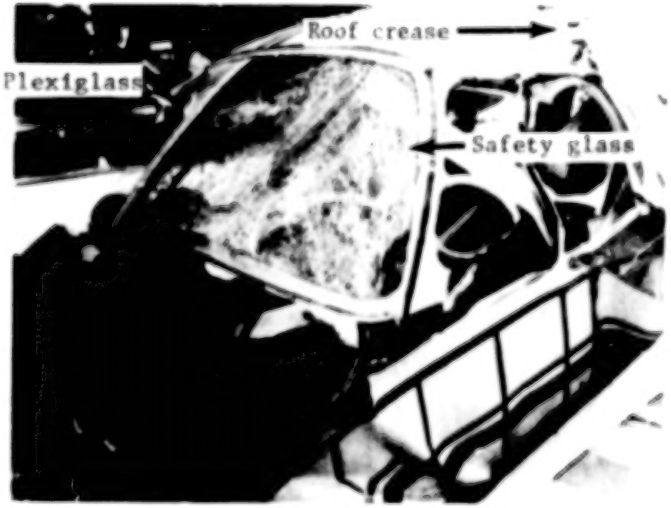

(d) Closeup view of cabin.

L-78-101

Figure 16.- Exterior damage to -45° test specimen.

(a) View of crew and cockpit.

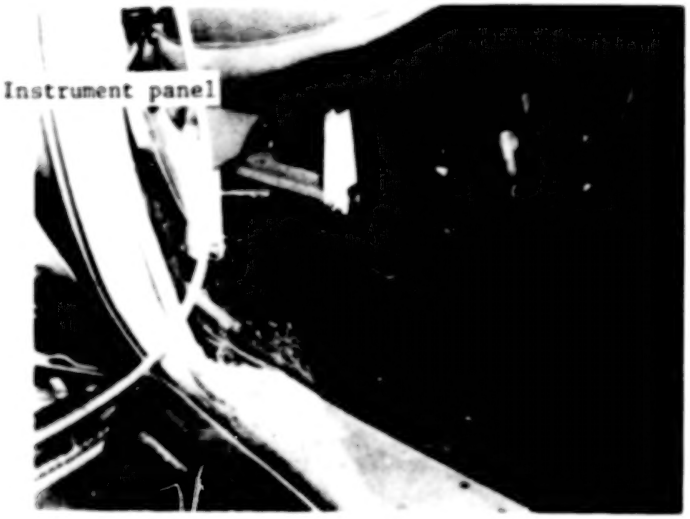

(b) Rear view of third-passenger seat.

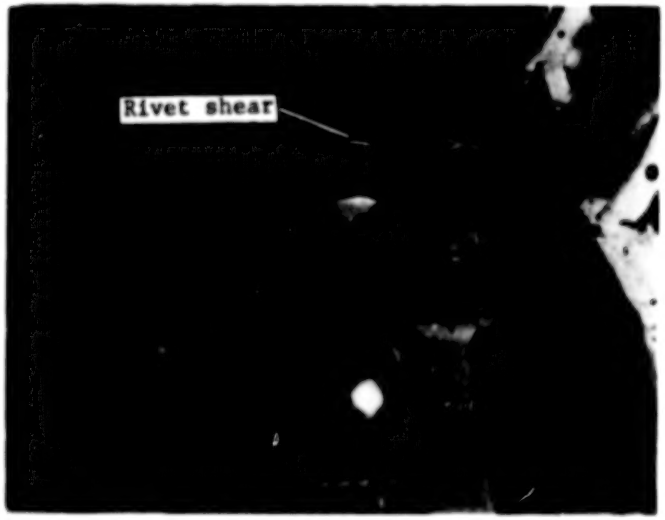

(c) Overall view of floor structure.

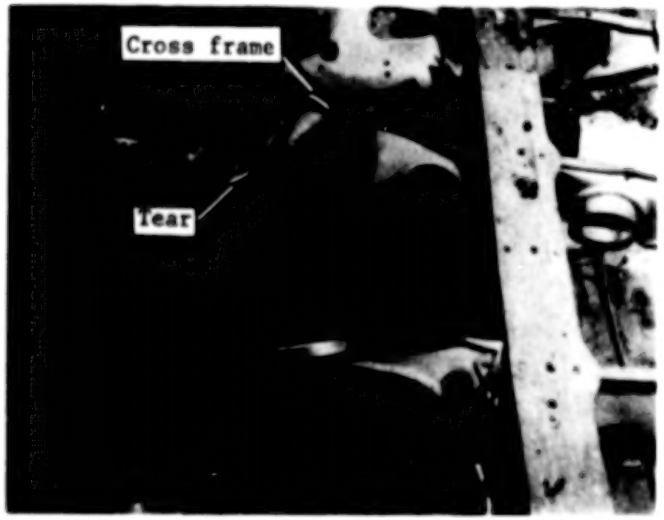

(d) Closeup view of floor structure.

L-78-102

Figure 17.- Interior damage to -45° test specimen.

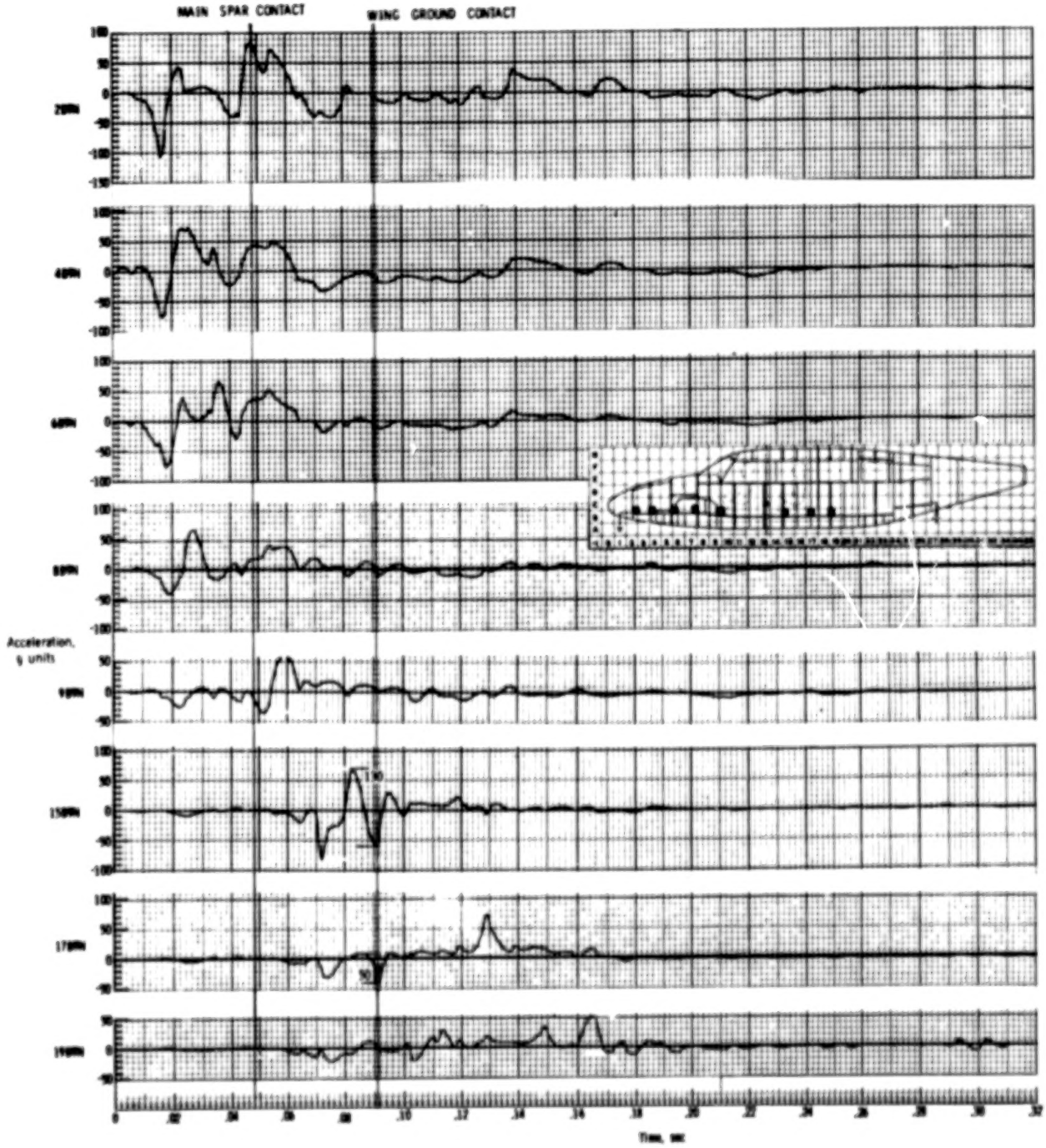

(a) -15° test specimen.

Figure 18.- Time histories of normal accelerations.

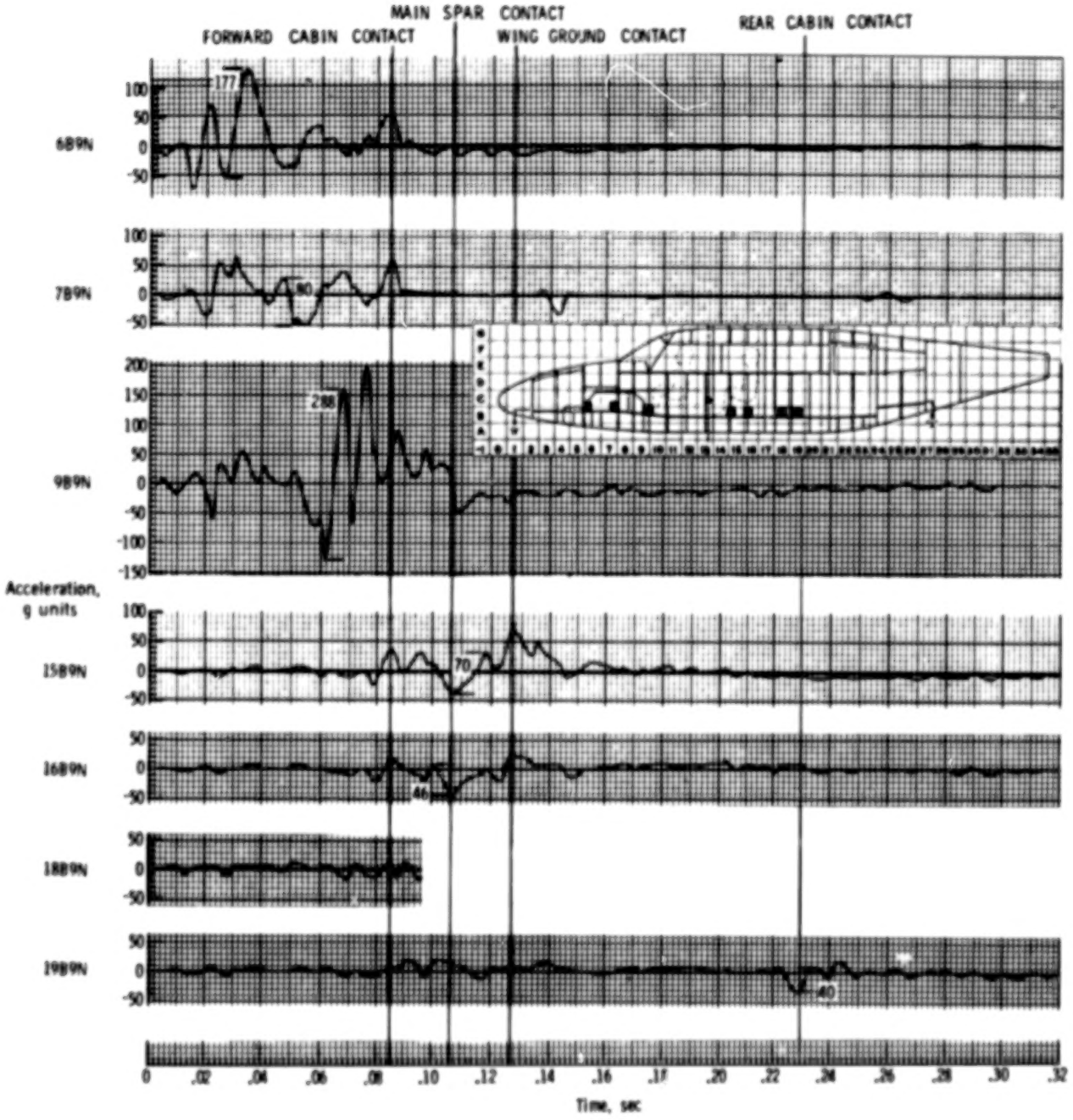

(b) -30° test specimen.

Figure 18.- Continued.

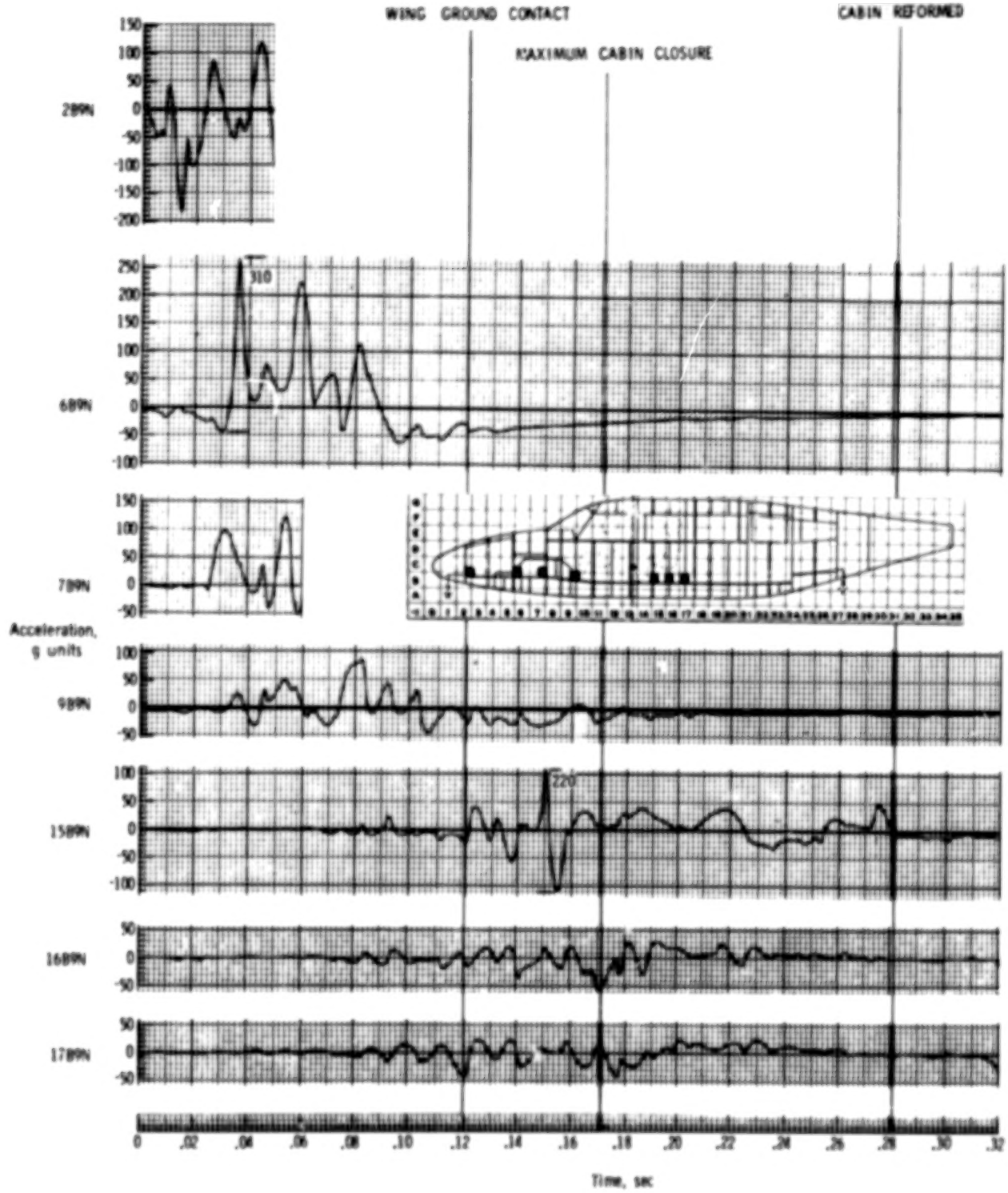

(c) -45° test specimen.

Figure 18.- Concluded.

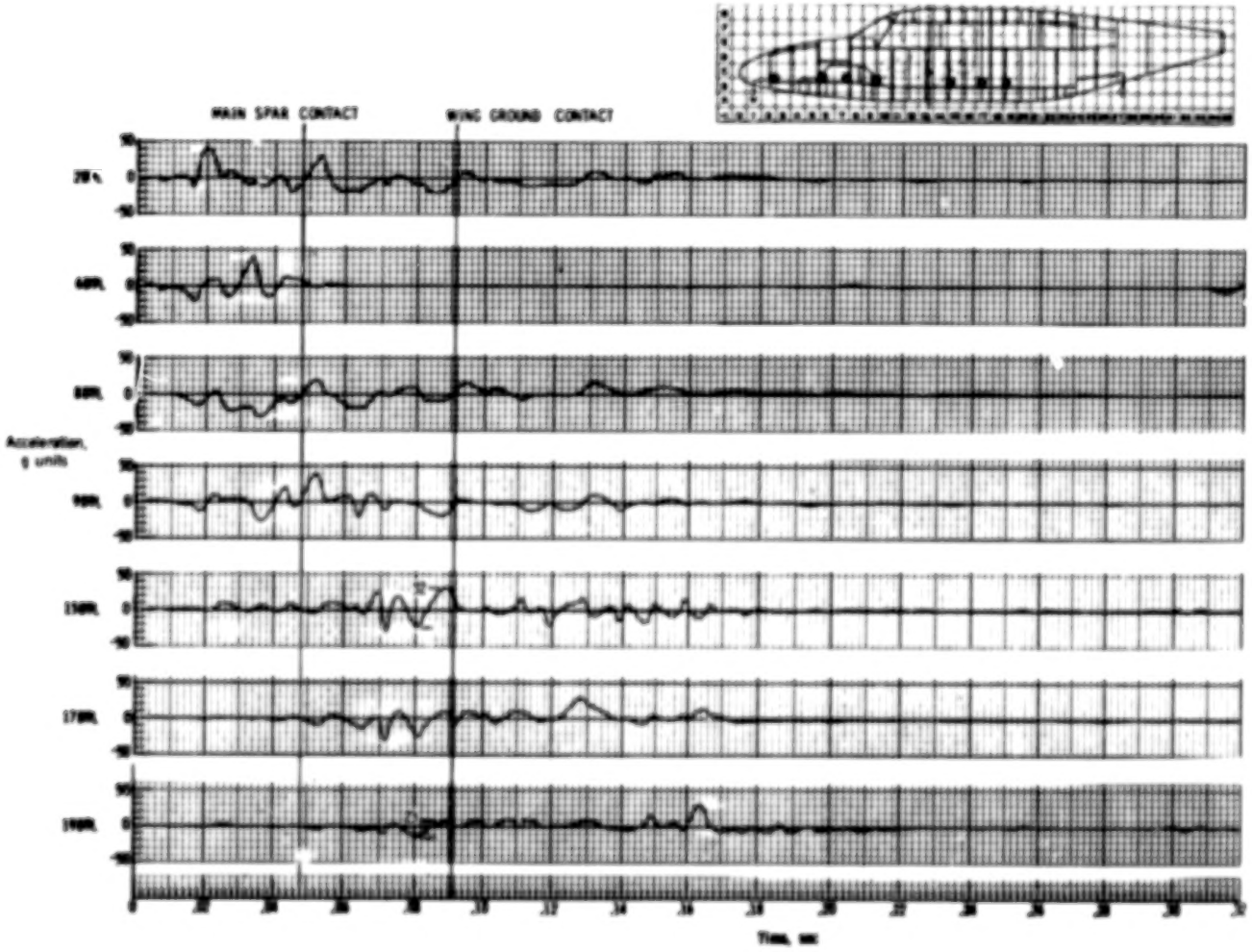

(a) -15° test specimen.

Figure 19.- Time histories of floor-beam longitudinal accelerations.

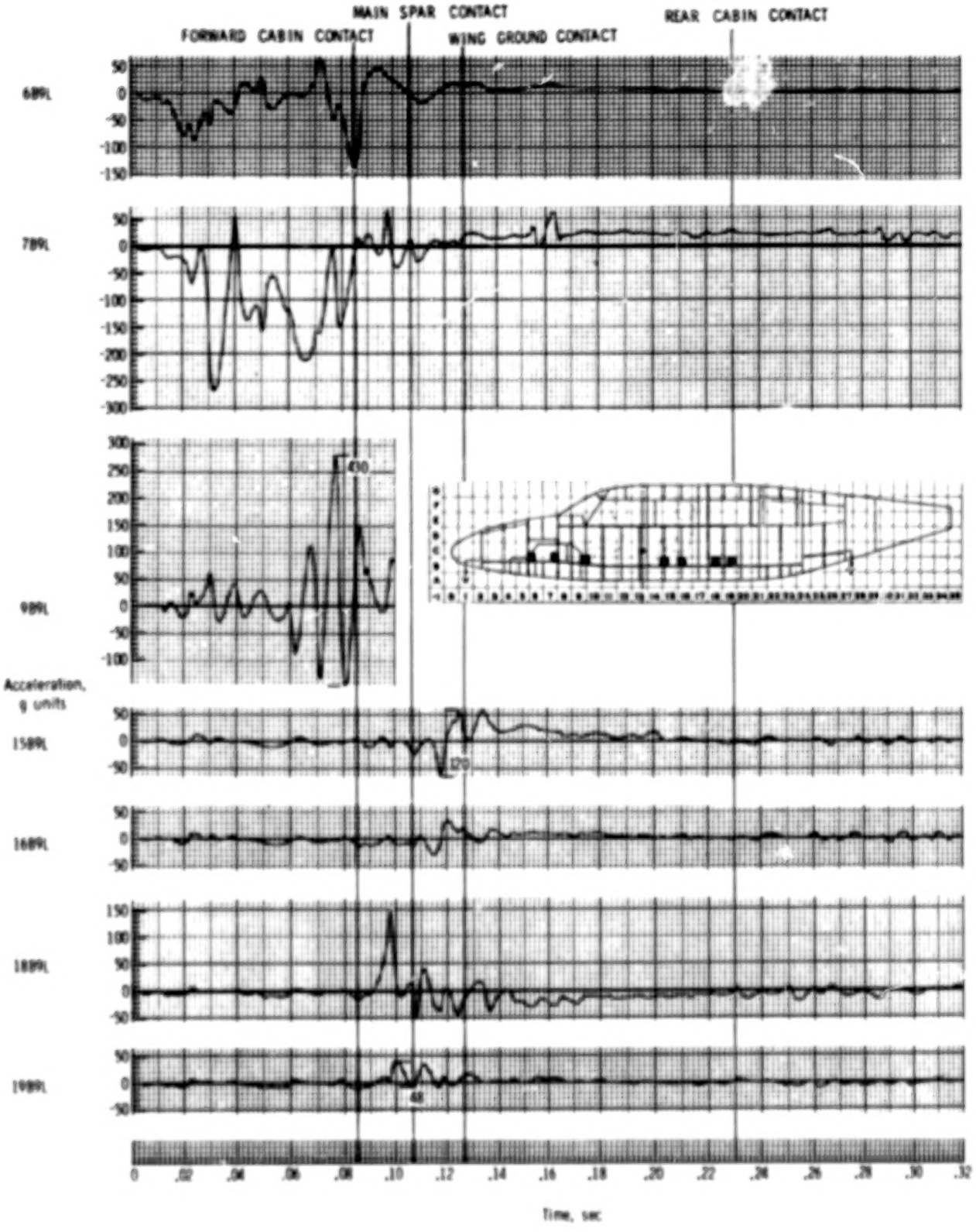

(b) -30° test specimen.

Figure 19.- Continued.

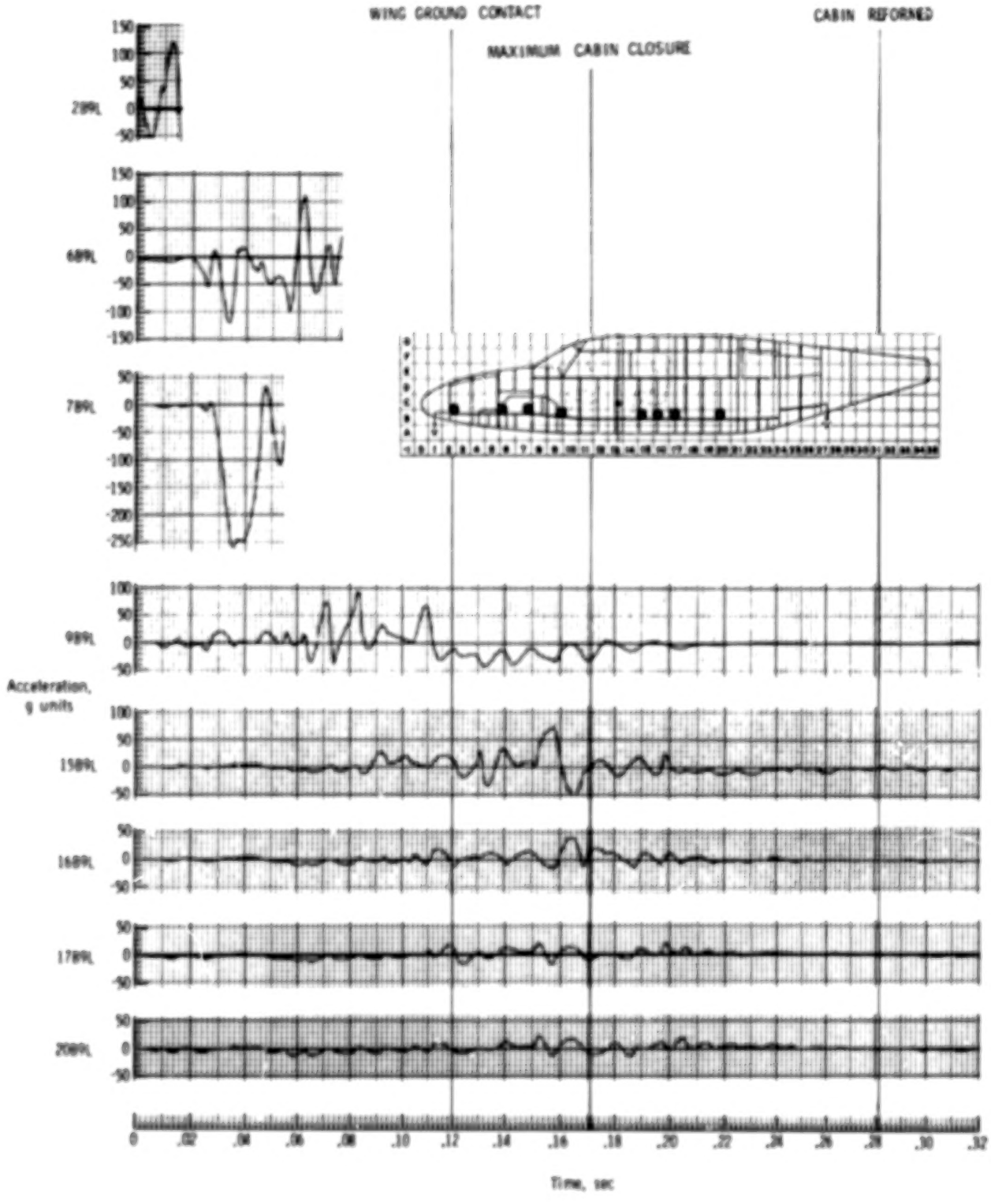

(c) -45° test specimen.

Figure 19.- Concluded.

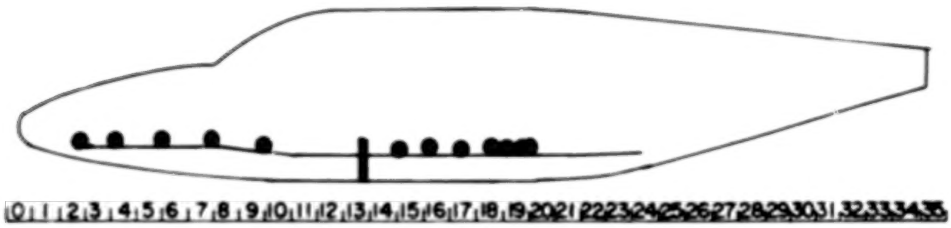

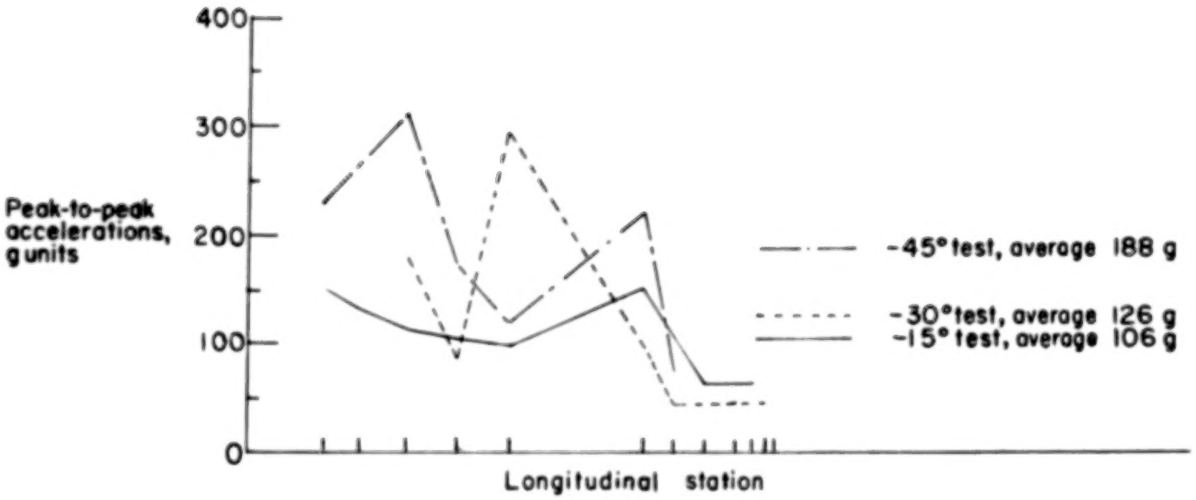

(a) Normal accelerations.

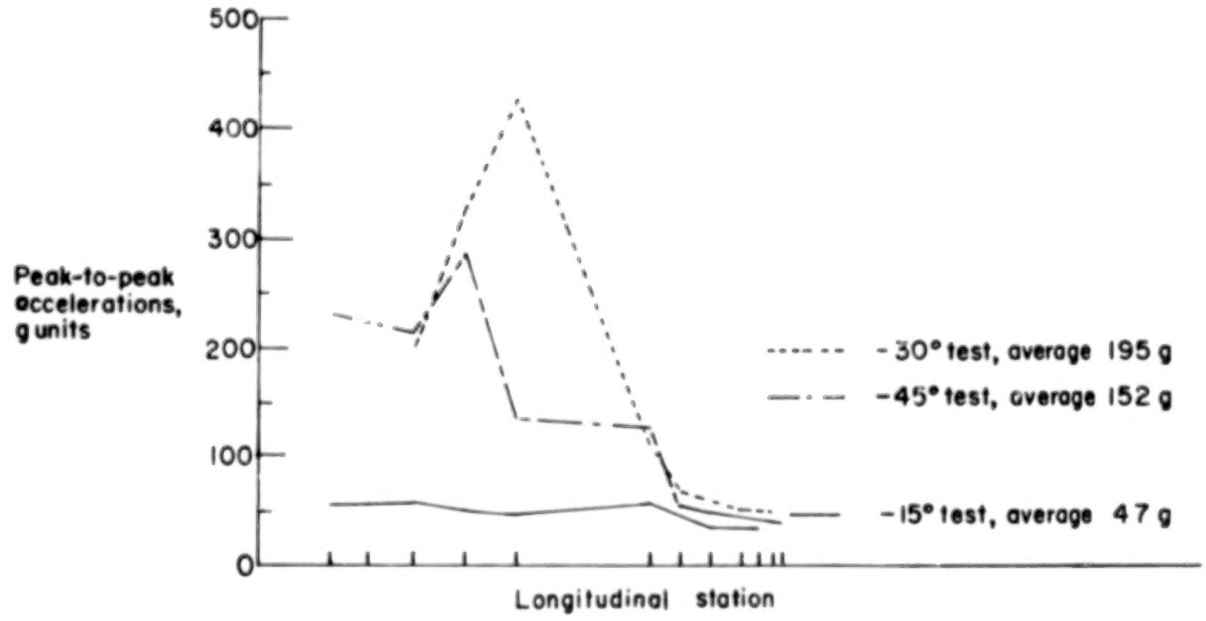

(b) Longitudinal accelerations.

Figure 20.- Peak-to-peak accelerations along floor beam.

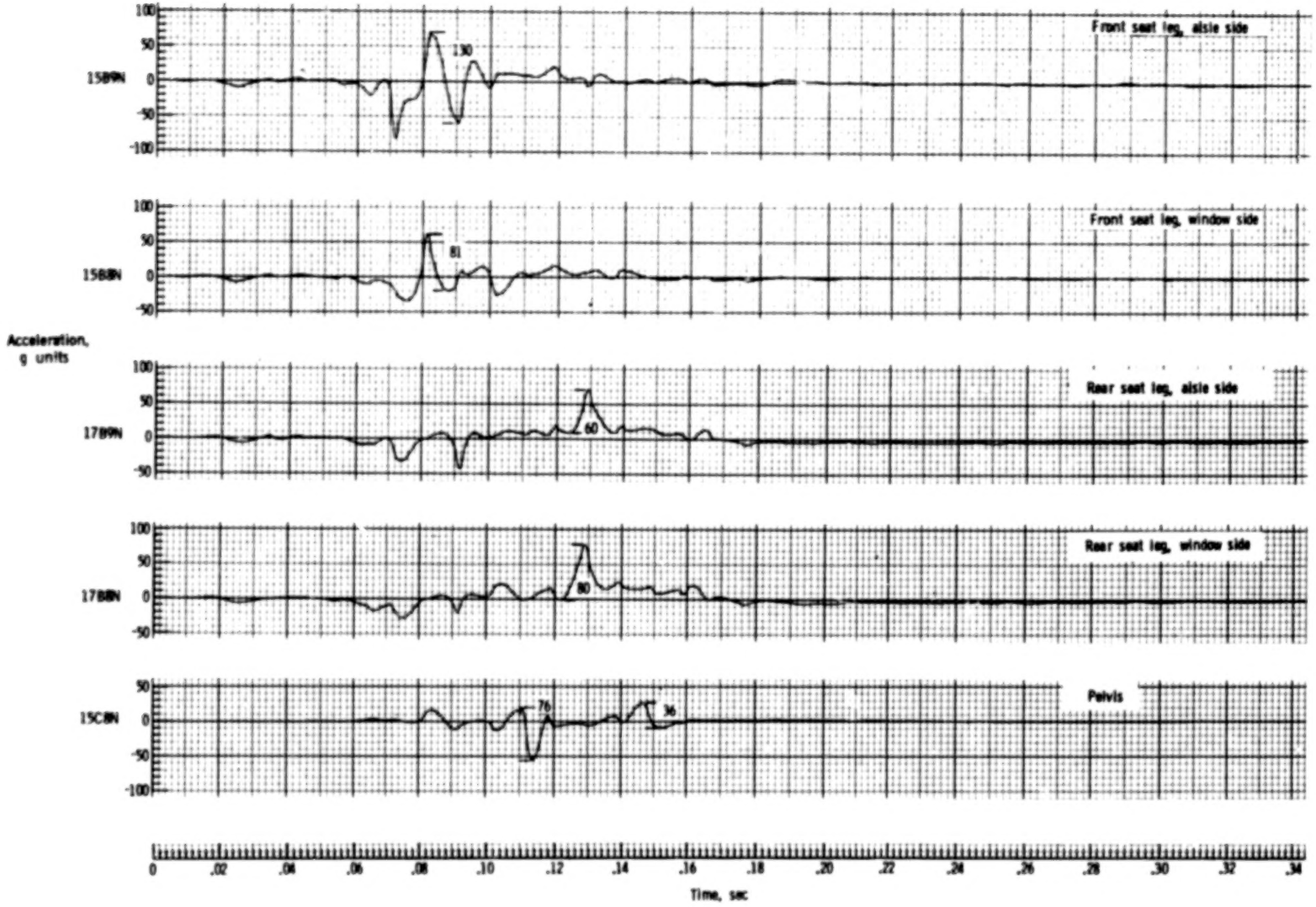

(a) -15° test specimen.

Figure 21.- Normal accelerations on floor and on dummy pelvis at first-passenger location.

2/0

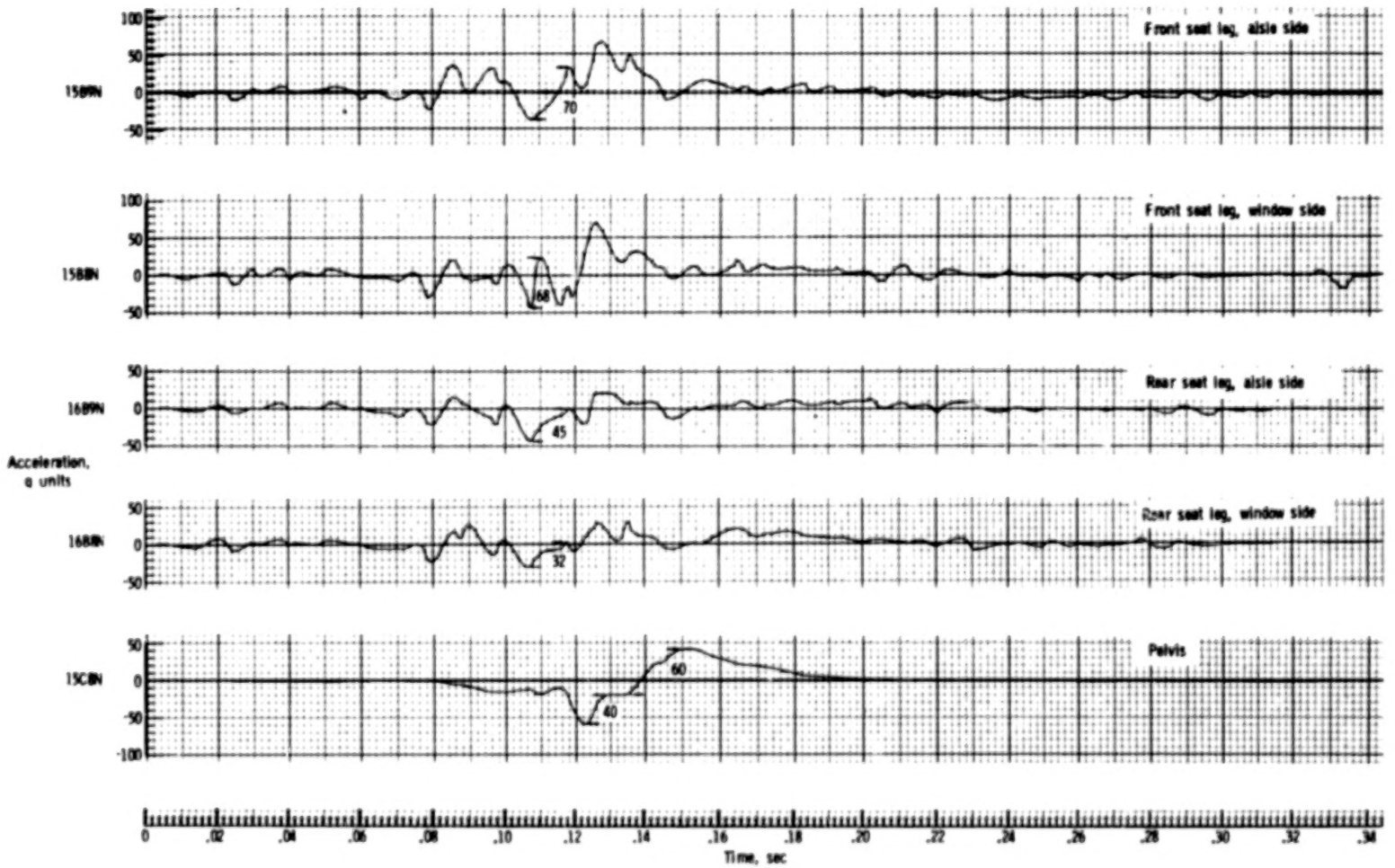

(b) -30° test specimen.

Figure 21.- Continued.

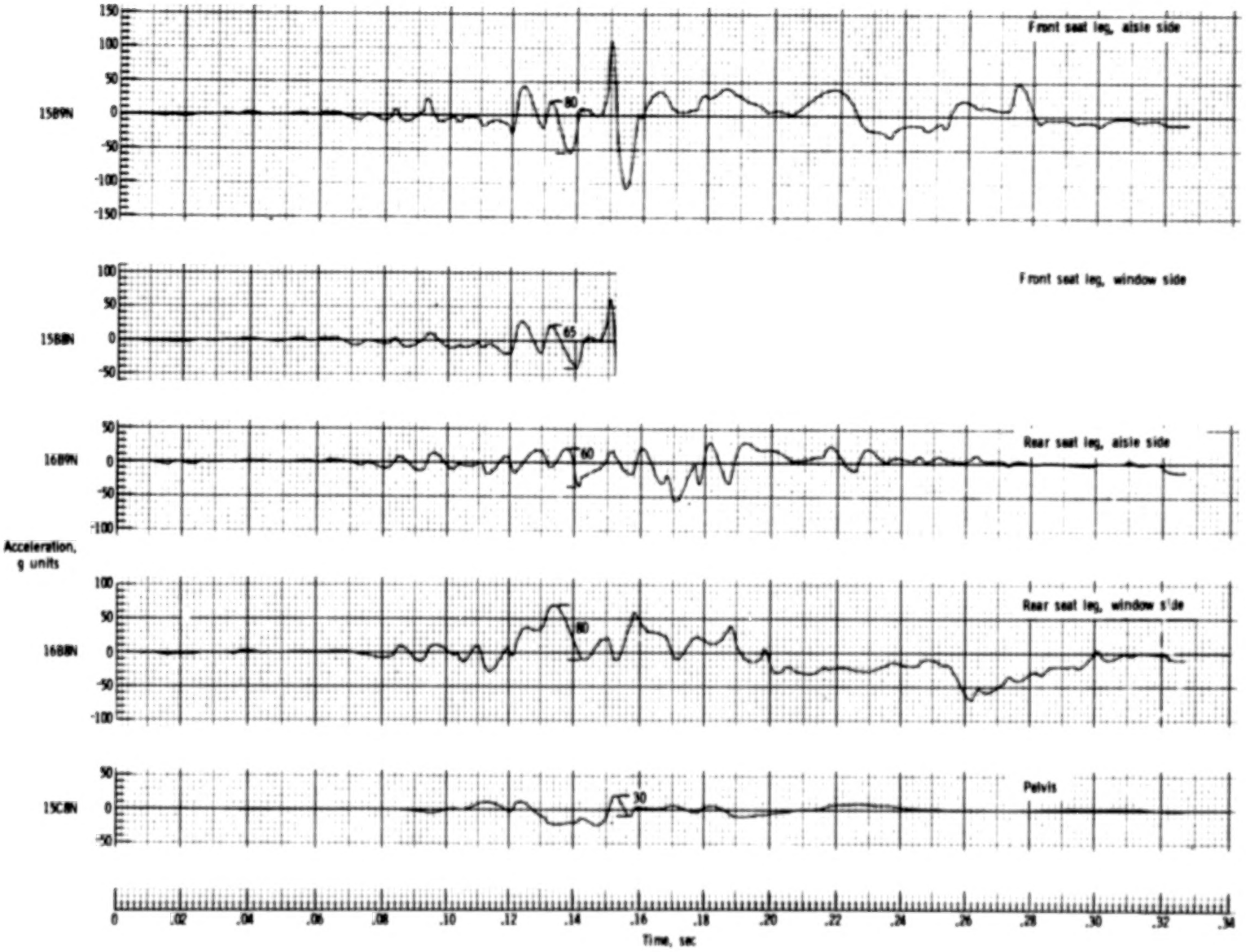

(c) -45° test specimen.

Figure 21.- Concluded.

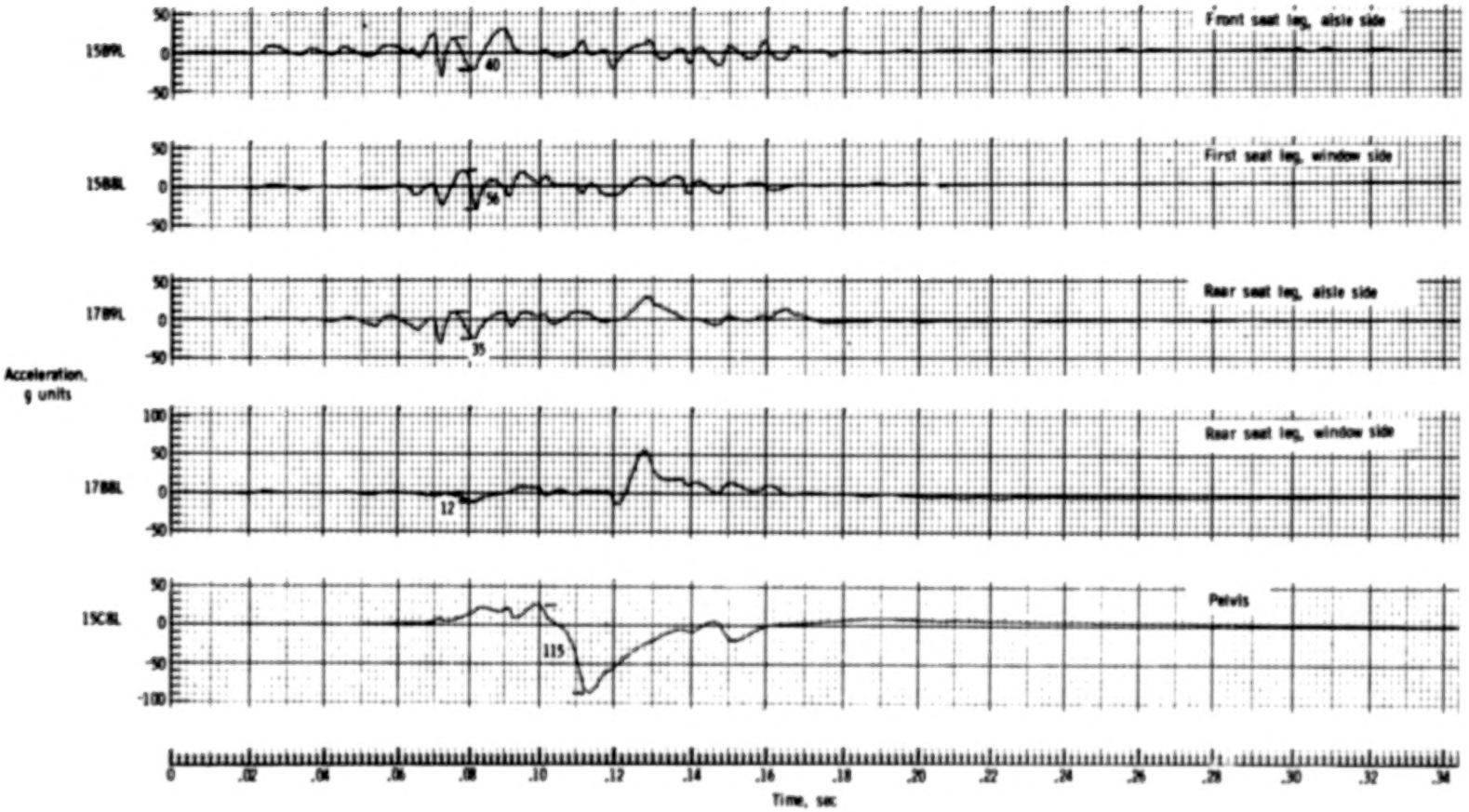

(a) -15° test specimen.

Figure 22.- Longitudinal accelerations on floor and on dummy pelvis at first-passenger location.

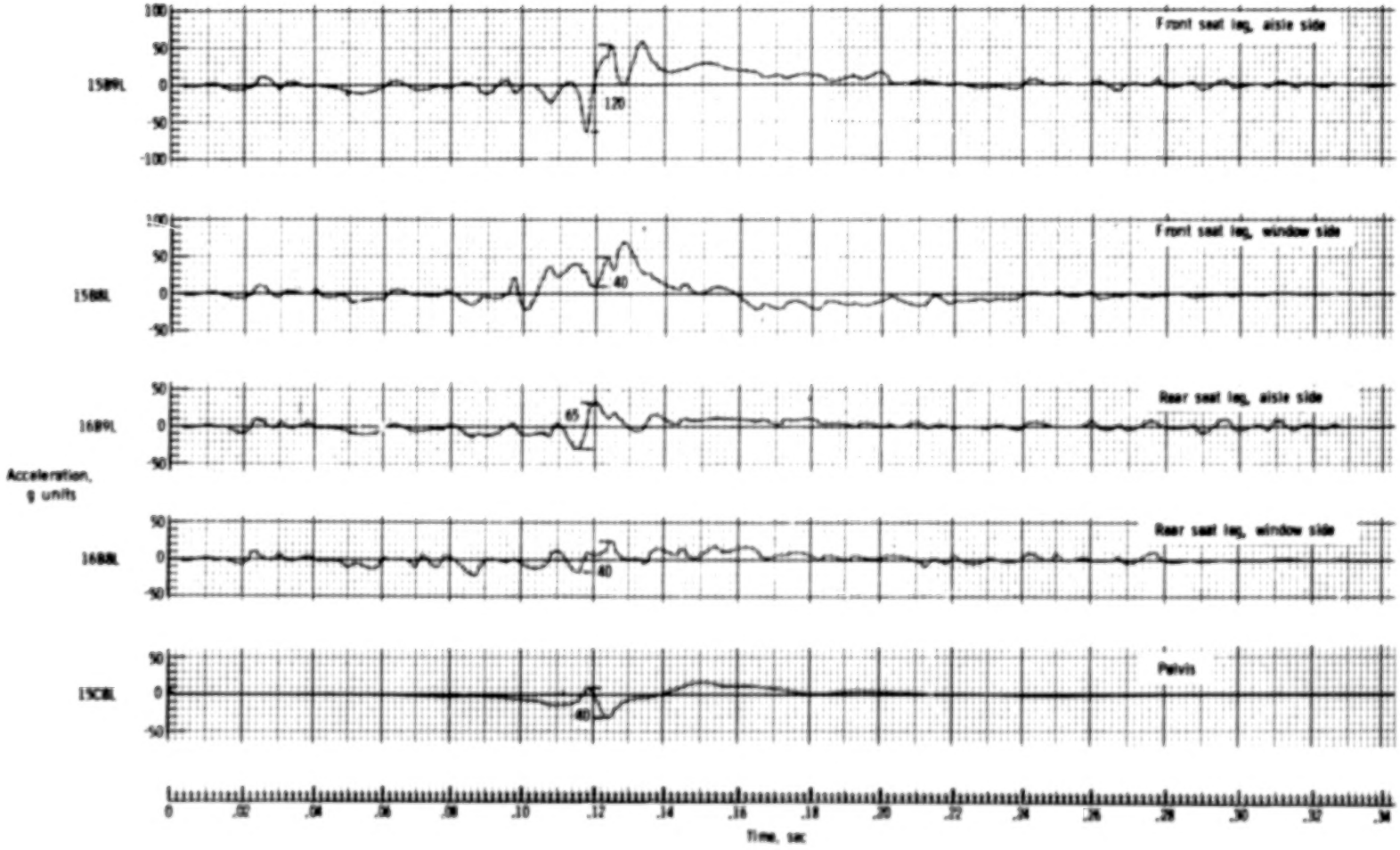

(b) -30° test specimen.

Figure 22.- Continued.

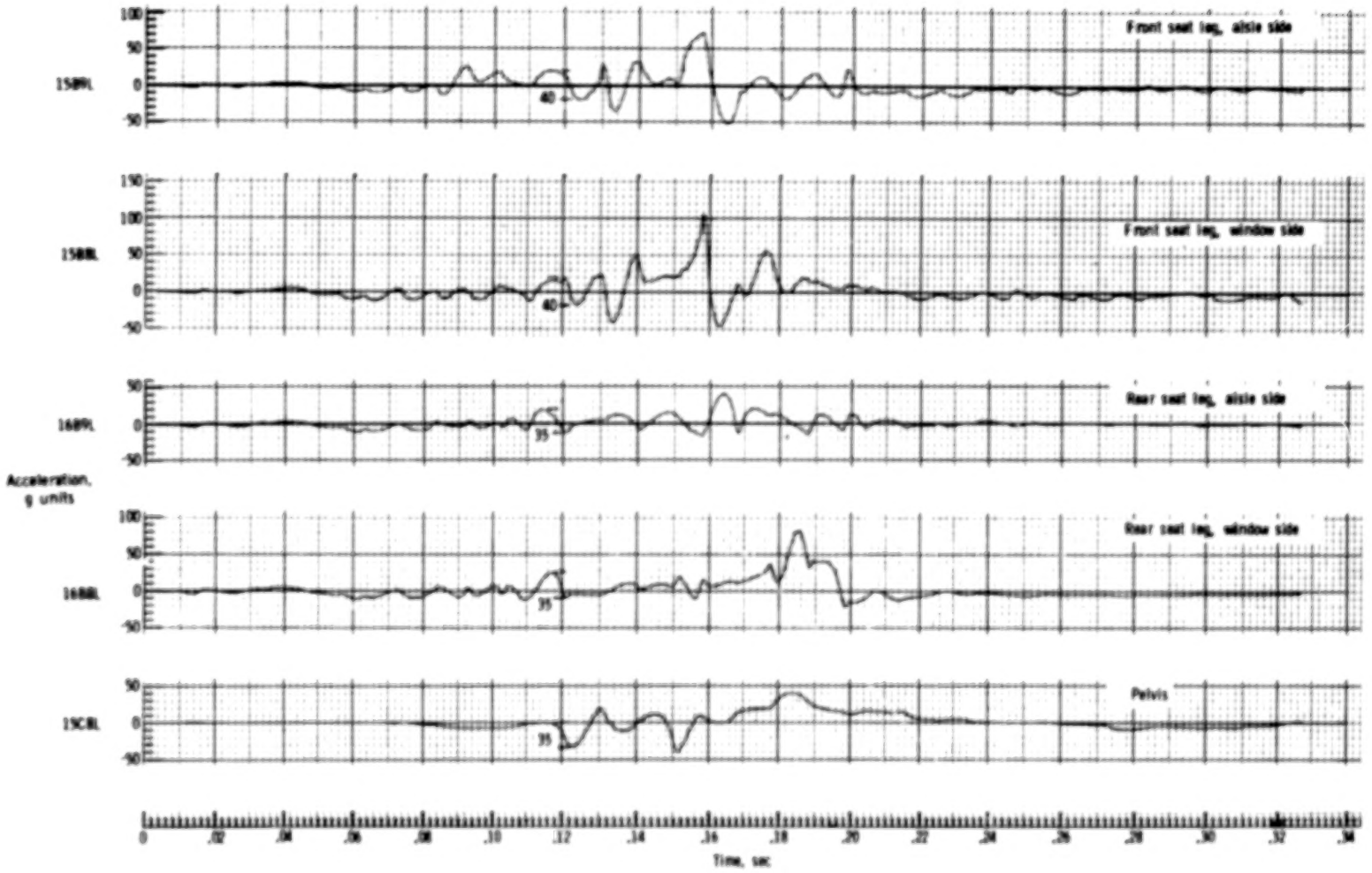

(c) -45° test specimen.

Figure 22.- Concluded.

45

APPENDIX

ACCELEROMETER DATA

Included in this appendix is the complete set of acceleration time histories for the three crash tests and a schematic to help determine the accelerometer locations corresponding to the time histories. (See figs. A1 to A4.)

The data have been passed through a 4- to 3300-Hz band-pass filter during recording and then digitized at 4000 samples per second. The digitized data were smoothed by a least-squares fit through every 50 points on a third-order polynomial and a 10-point overlap for continuity.

The data are grouped according to the accelerometer location and orientation. The accelerometer location is represented in the schematic by a coordinate system in the x-, z-, and y-directions. The accelerometer normal, longitudinal, and transverse orientations are indicated on the traces by N, L, and T, respectively. Thus, the first accelerometer adjacent to the floor beam in the normal direction is represented by 2B9N. Each station block along the X-, Z-, and Y-axes is 25.4 cm in length.

On the data plots, the abscissa represents elapsed time in seconds. Zero time is the time at initial contact, that is, the time at which the fuselage first contacted the impact surface. The accelerations in the ordinate are expressed in g units and each trace is identified by the location and orientation of the recording accelerometer.

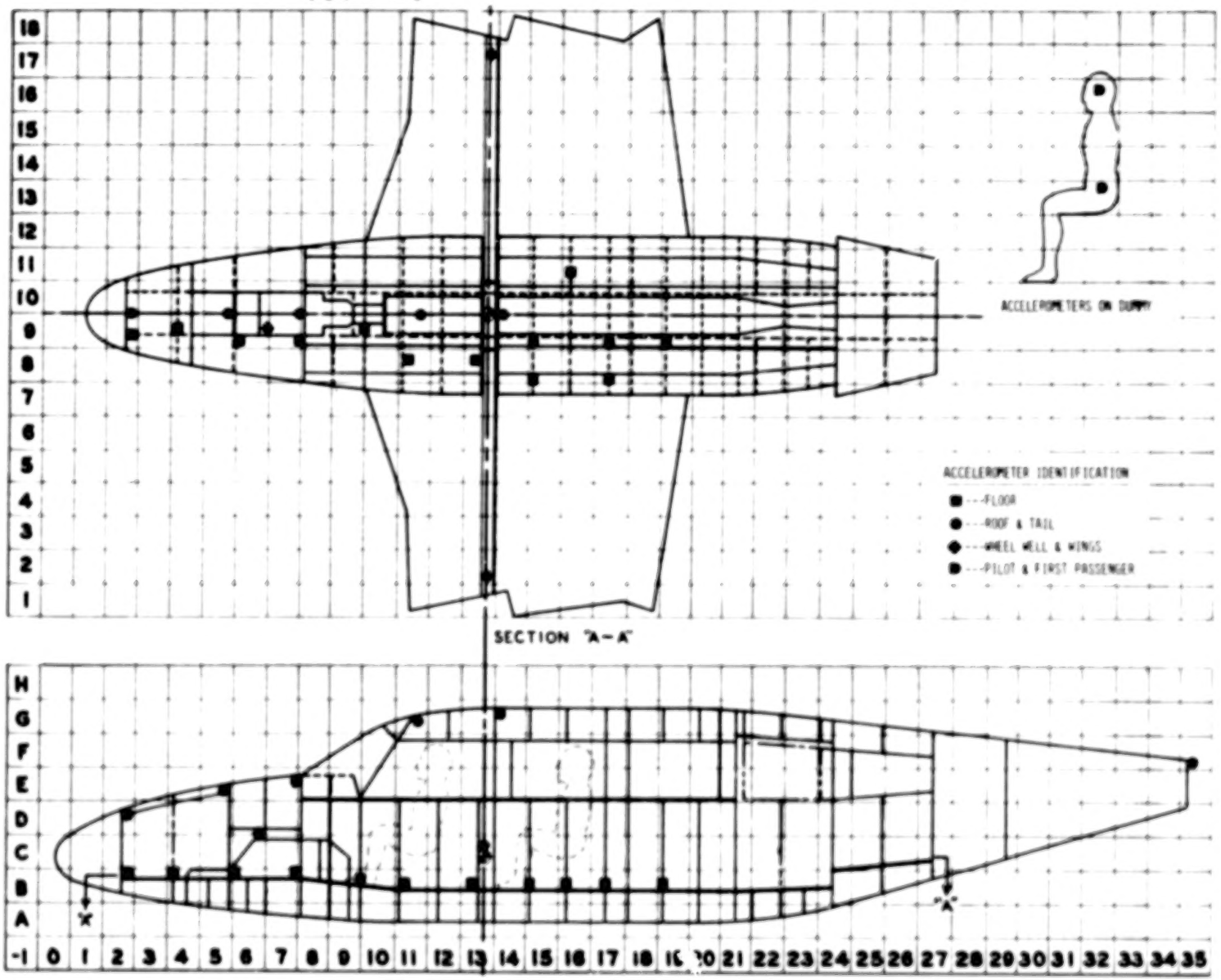

Figure A1.- Accelerometer locations (typical).

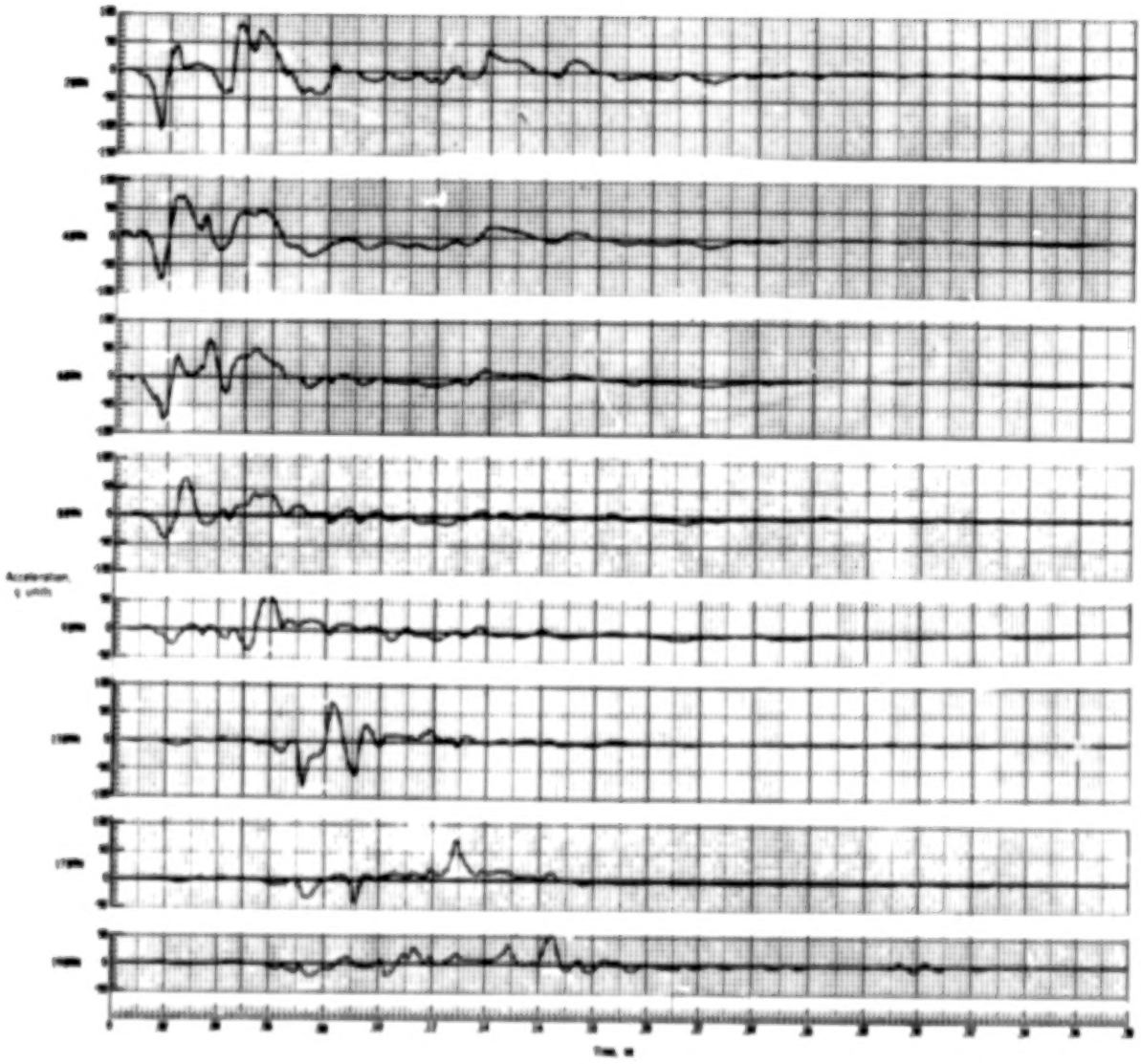

(a) Normal accelerations adjacent to floor beam.

Figure A2.- Acceleration time histories for -15° test specimen.

(b) Longitudinal accelerations adjacent to floor beam.

Figure A2.- Continued.

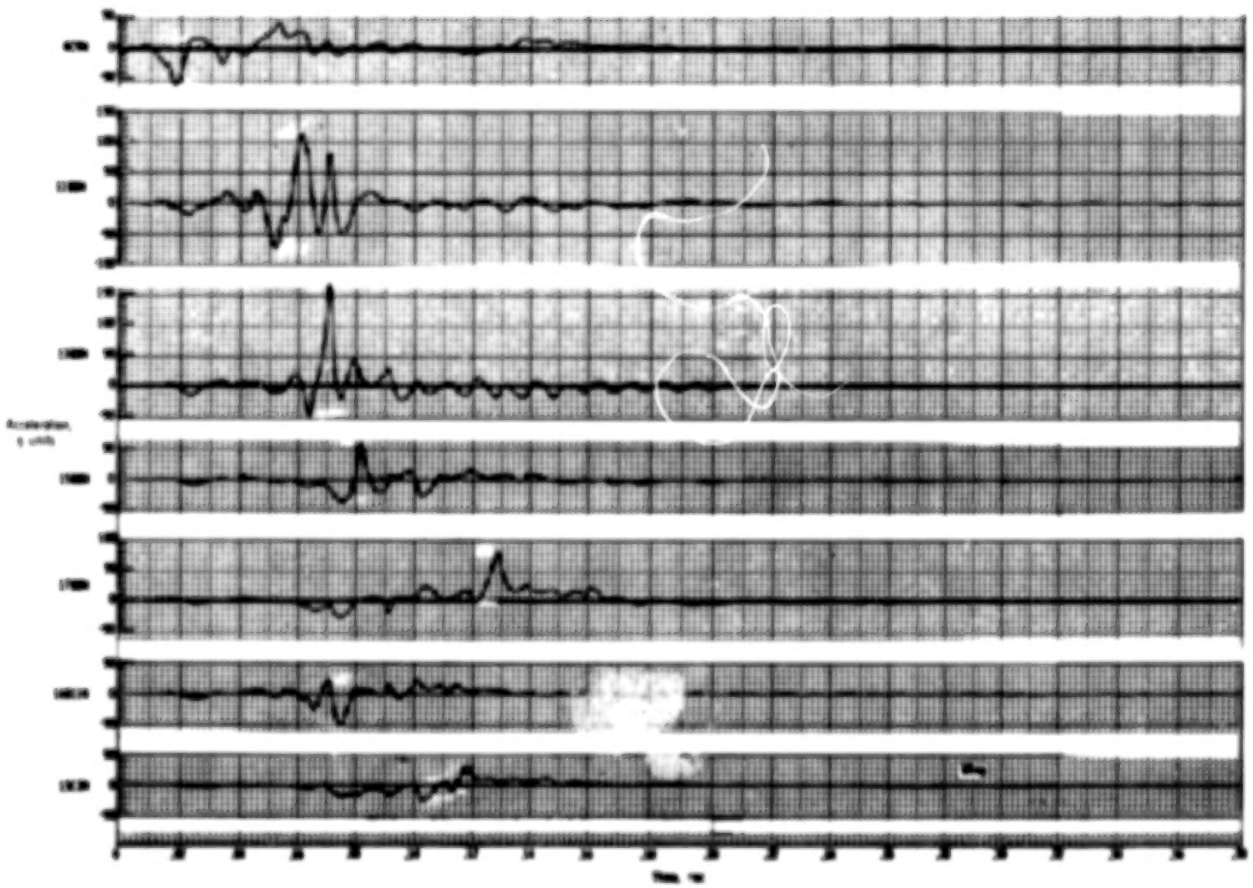

(c) Normal accelerations on cabin floor and wing.

Figure A2.- Continued.

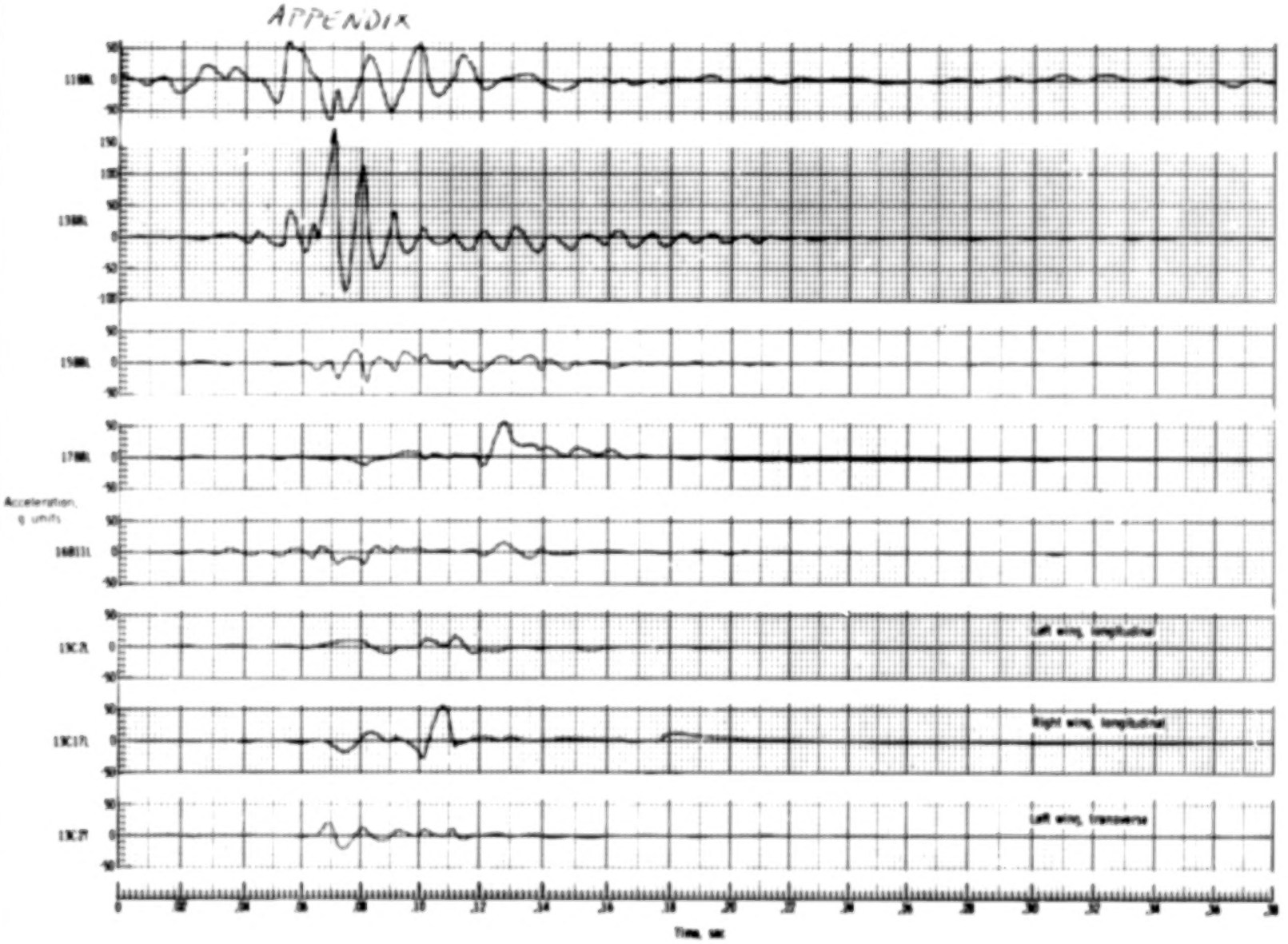

(d) Longitudinal accelerations on cabin floor and other accelerations.

Figure A2.- Continued.

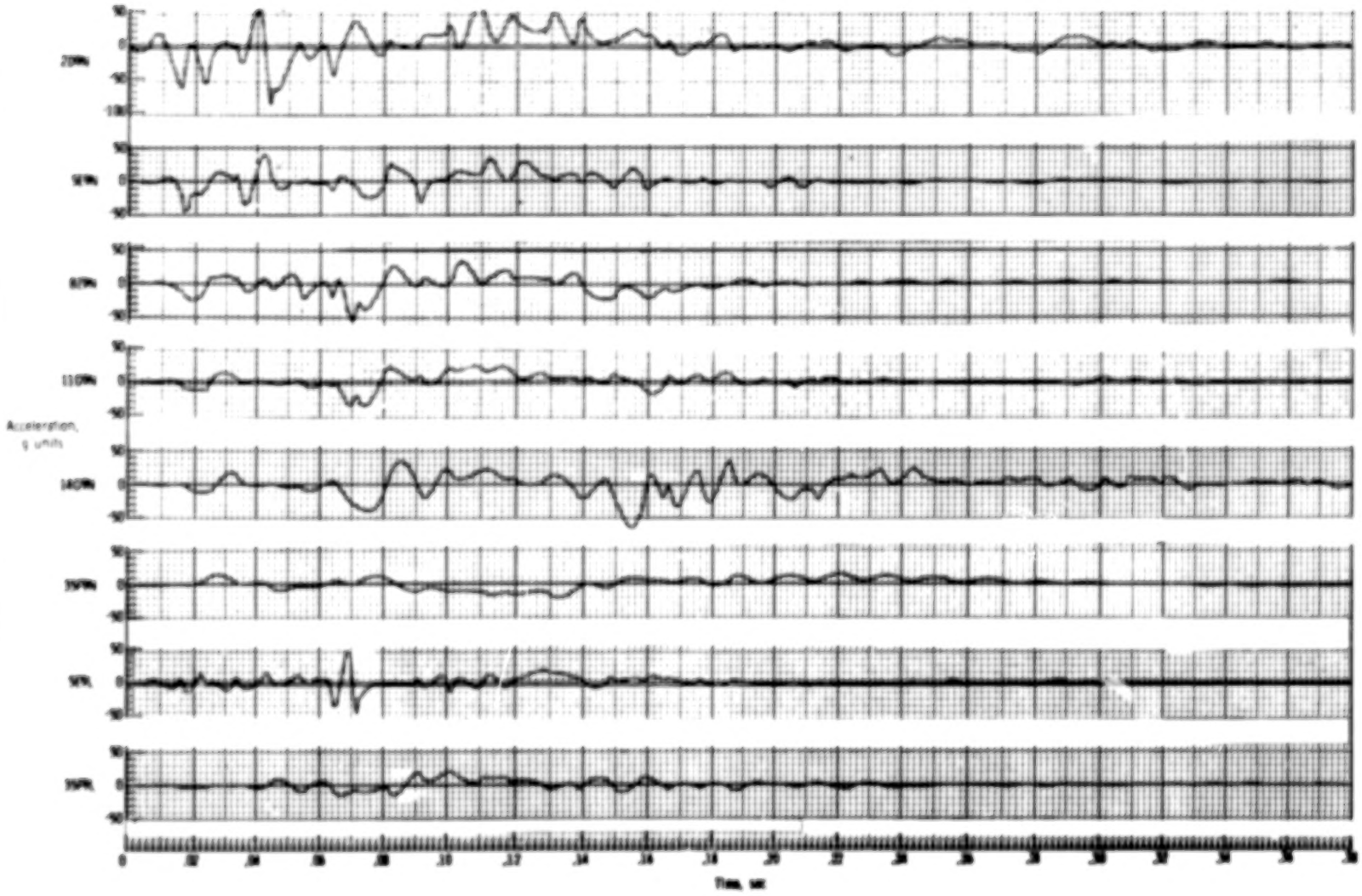

(e) Normal and longitudinal accelerations on roof.

Figure A2.- Continued.

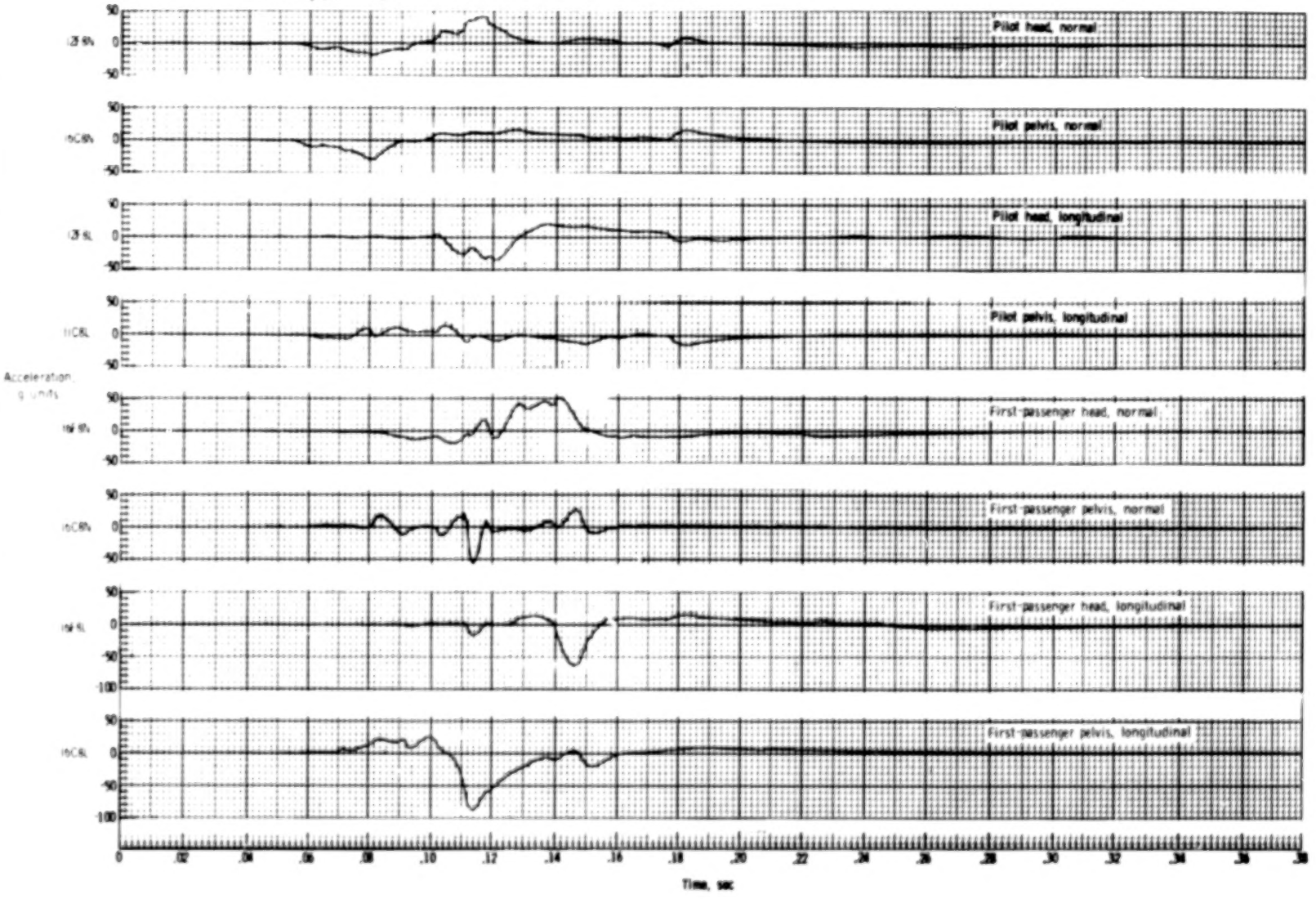

(f) Accelerations on pilot and first passenger.

Figure A2.- Concluded.

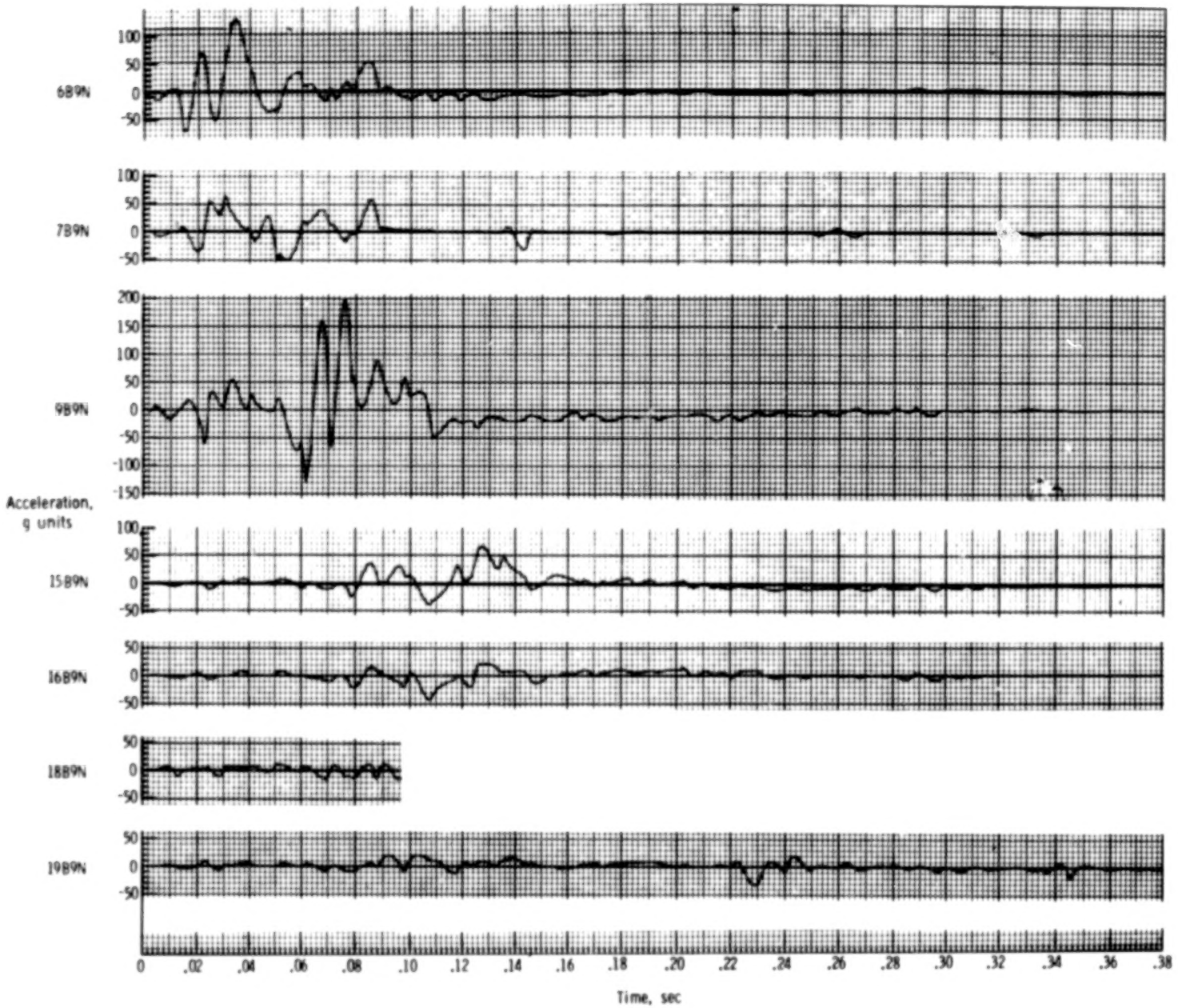

(a) Normal accelerations adjacent to floor beam.

Figure A3.- Acceleration time histories for -30° test specimen.

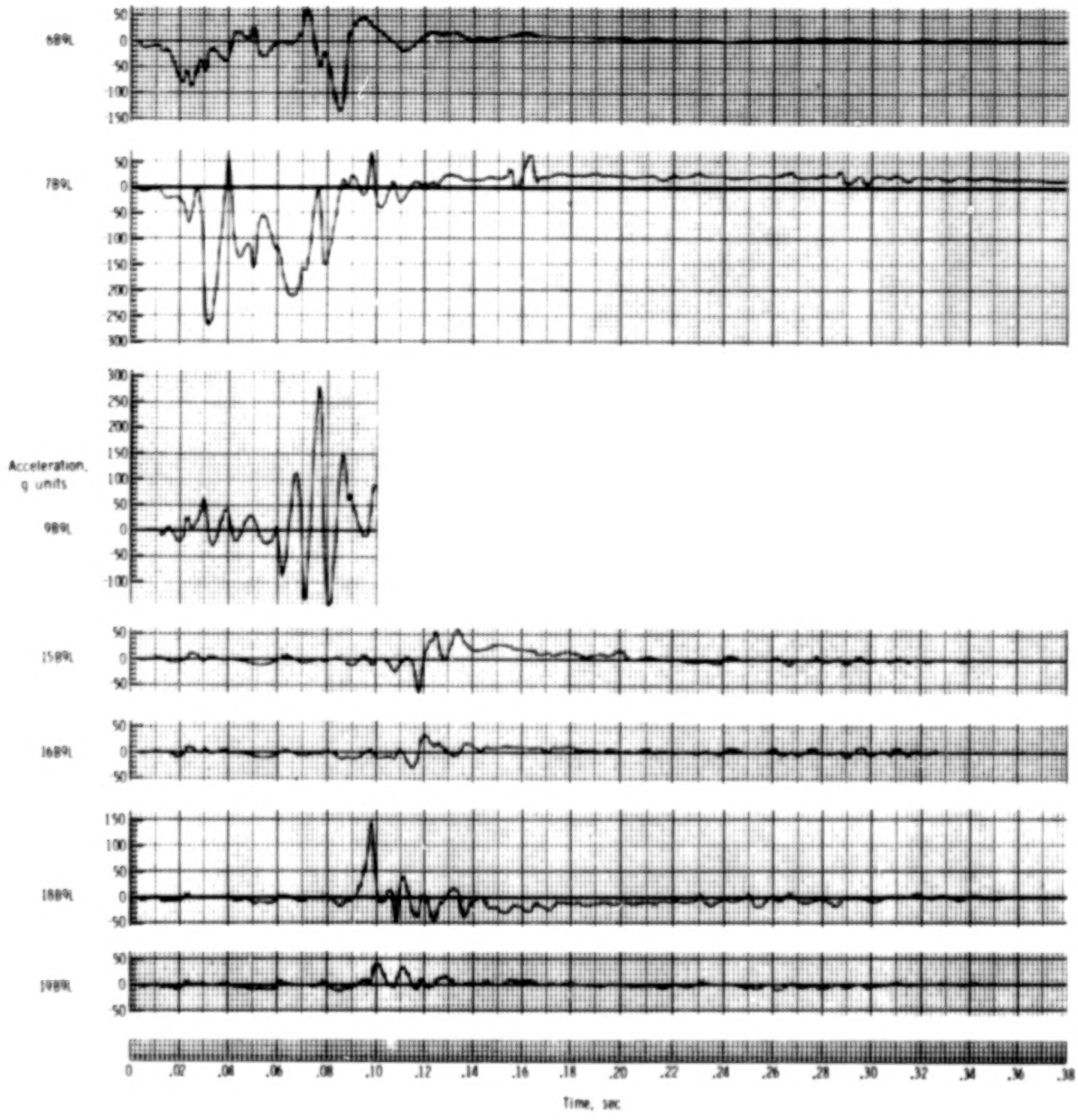

(b) Longitudinal accelerations adjacent to floor beam.

Figure A3.- Continued.

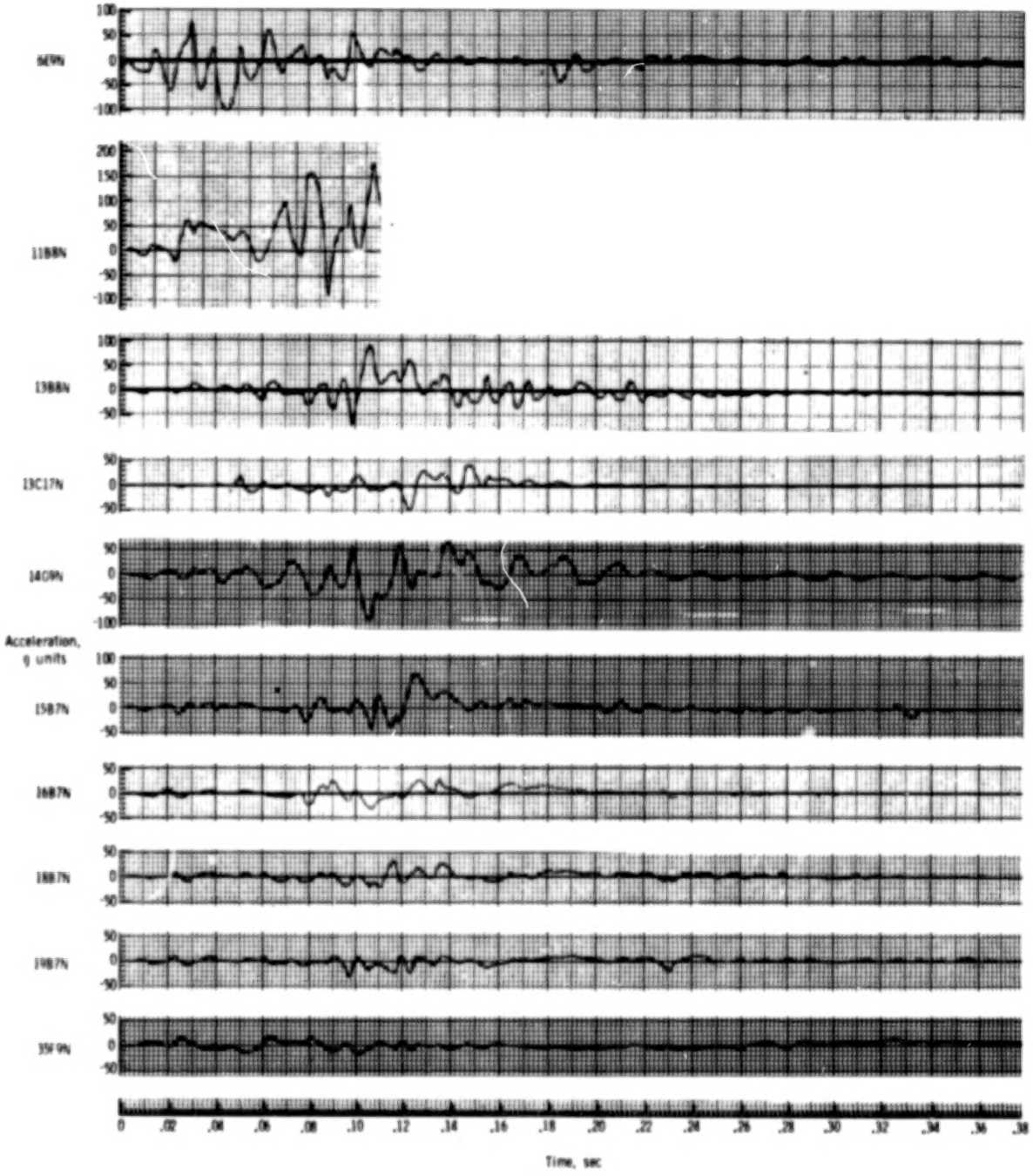

(c) Remaining normal structural accelerations.

Figure A3.- Continued.

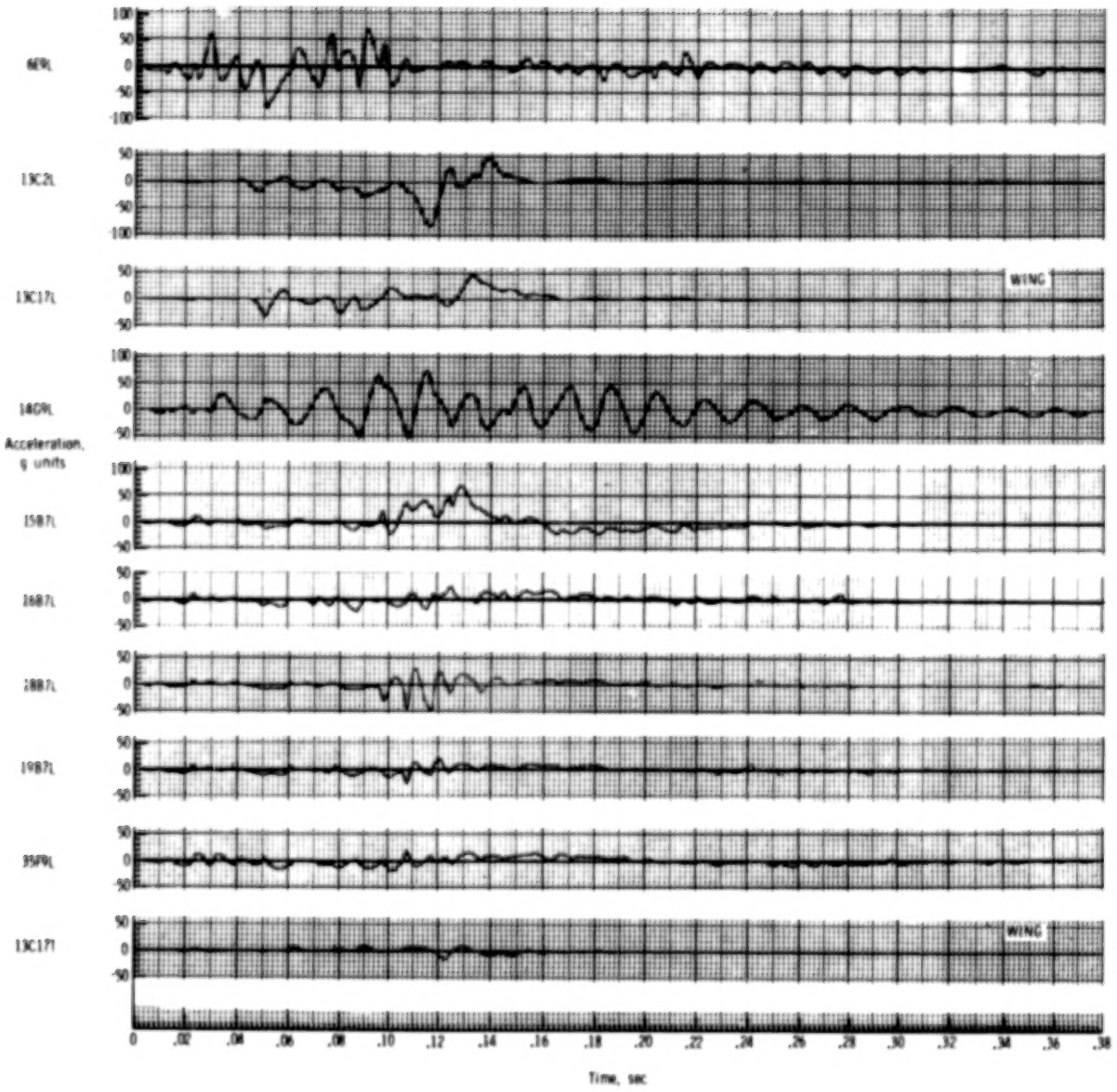

(d) Remaining longitudinal structural accelerations.

Figure A3.- Continued.

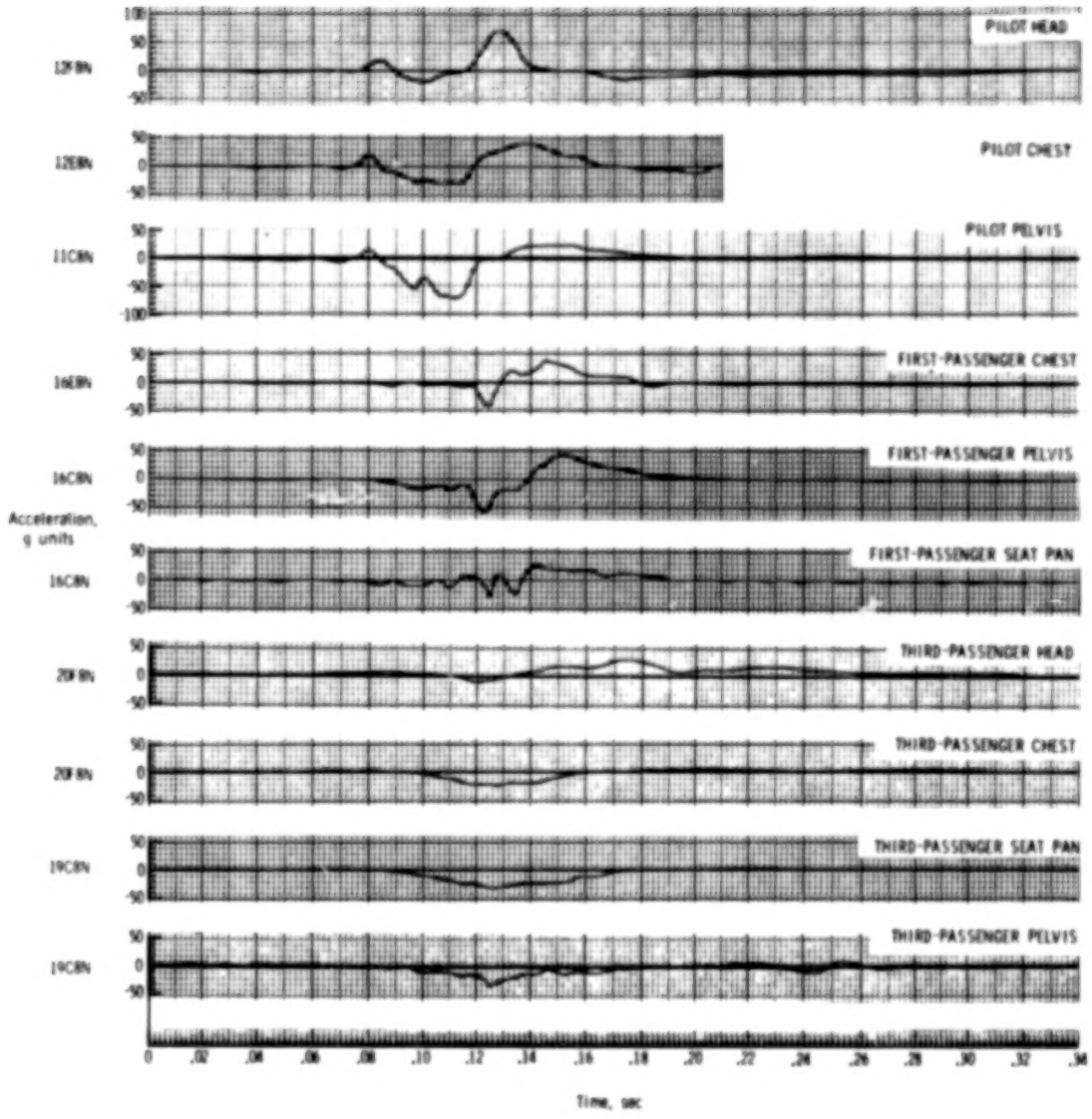

(e) Normal accelerations in dummies and on seats.

Figure A3.- Continued.

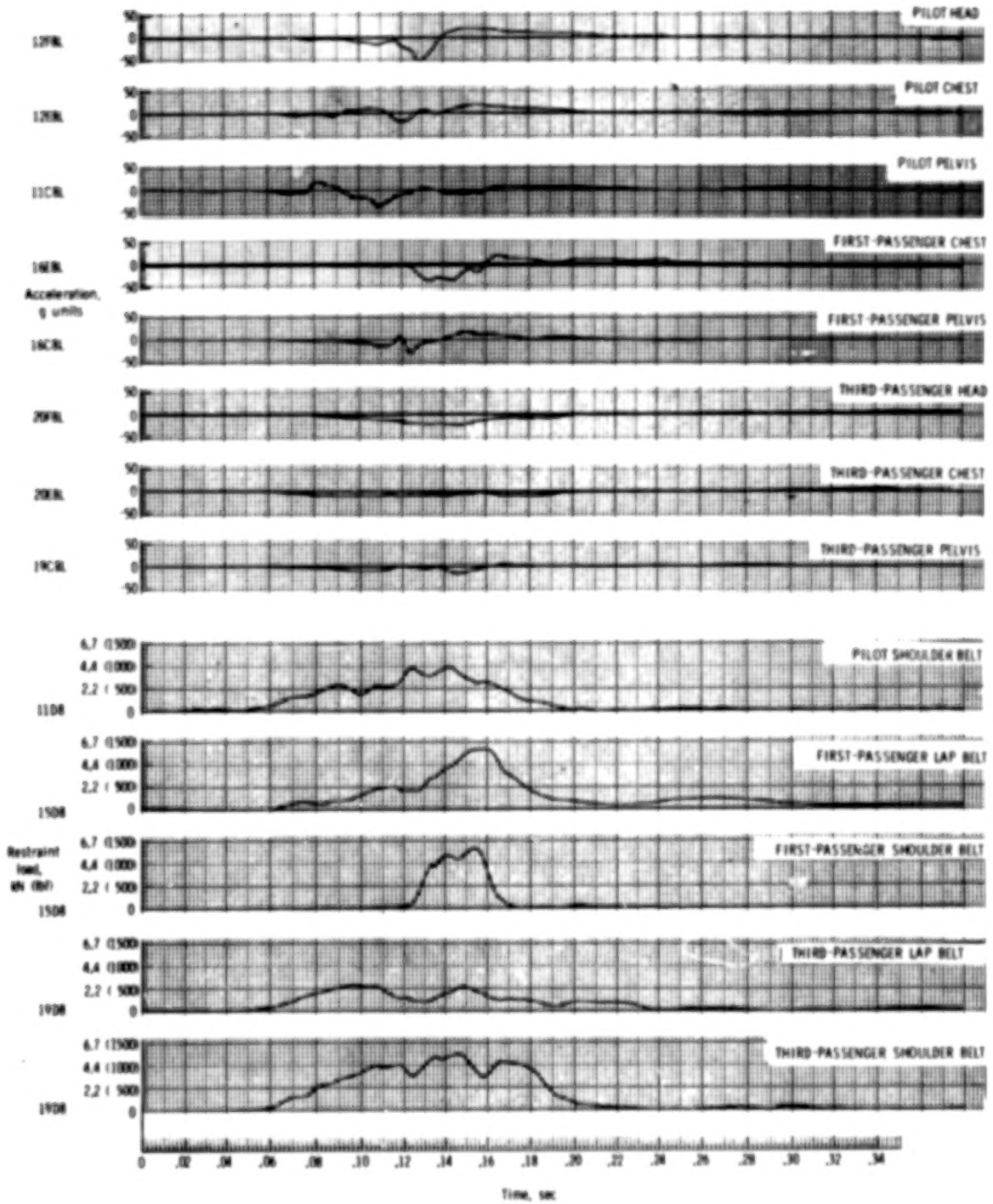

(f) Longitudinal accelerations in dummies and restraint system.

Figure A3.- Concluded.

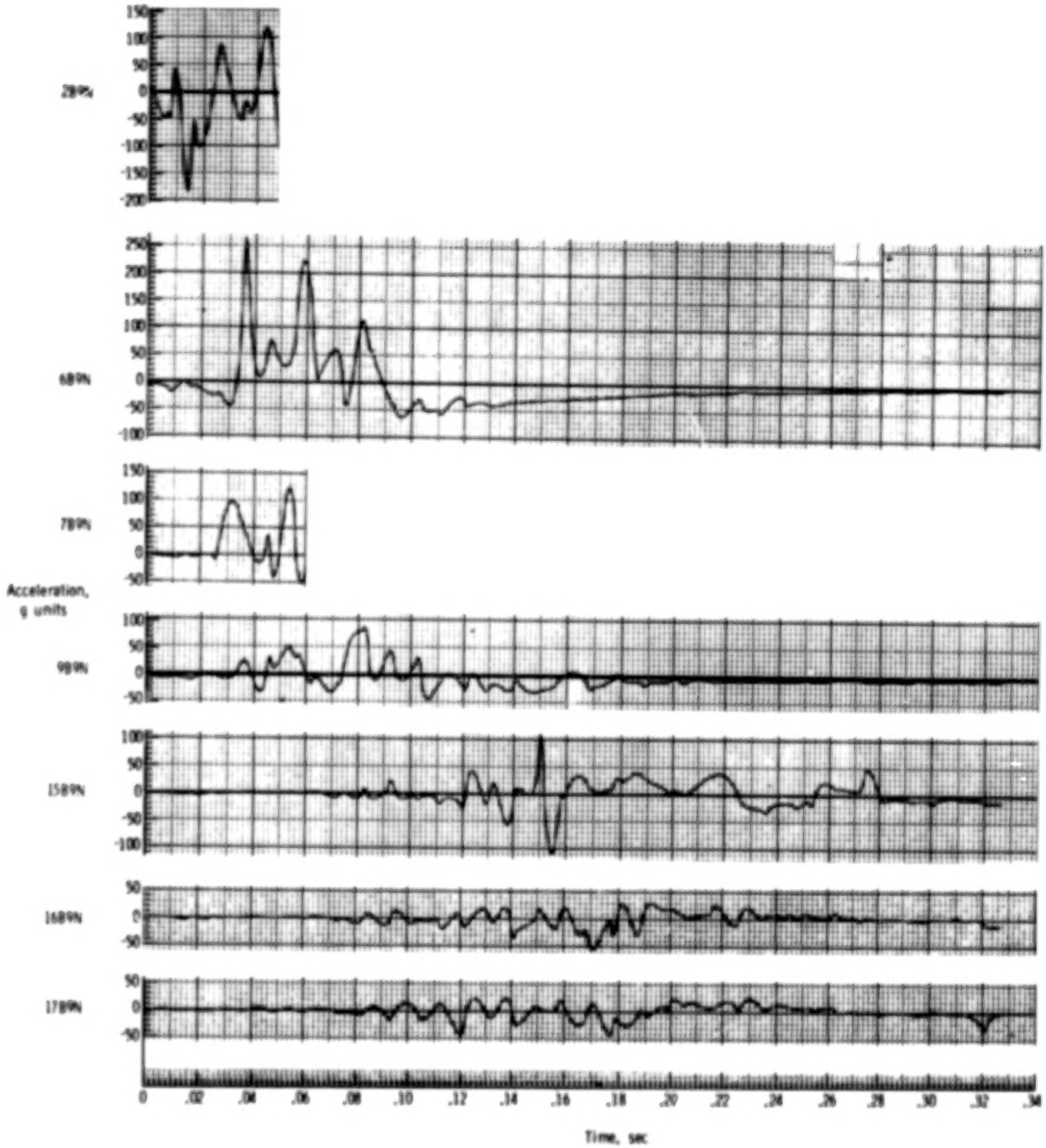

(a) Normal accelerations adajcent to floor beam.

Figure A4.- Acceleration time histories for -45° test specimen.

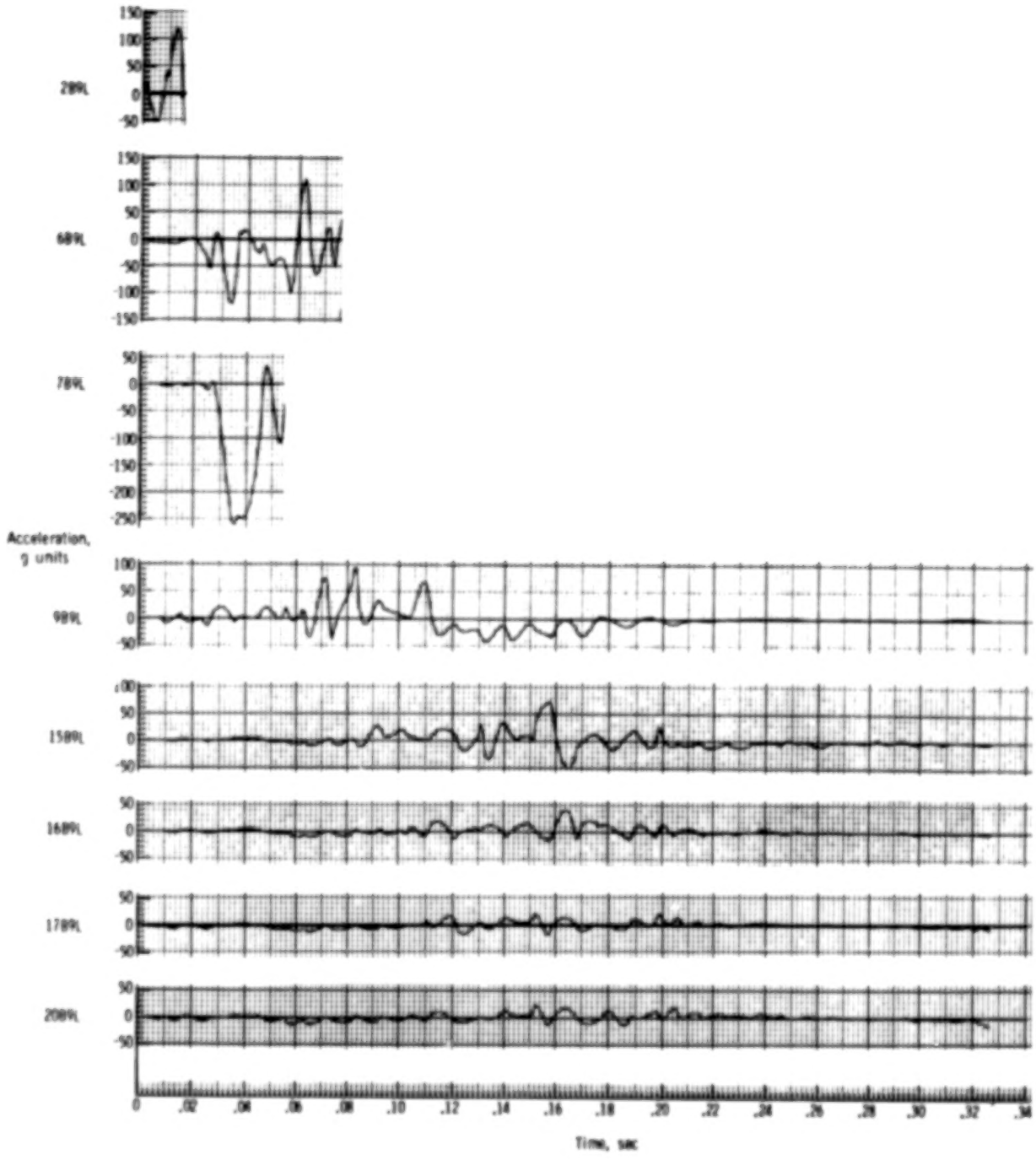

(b) Longitudinal accelerations adjacent to floor beam.

Figure A4.- Continued.

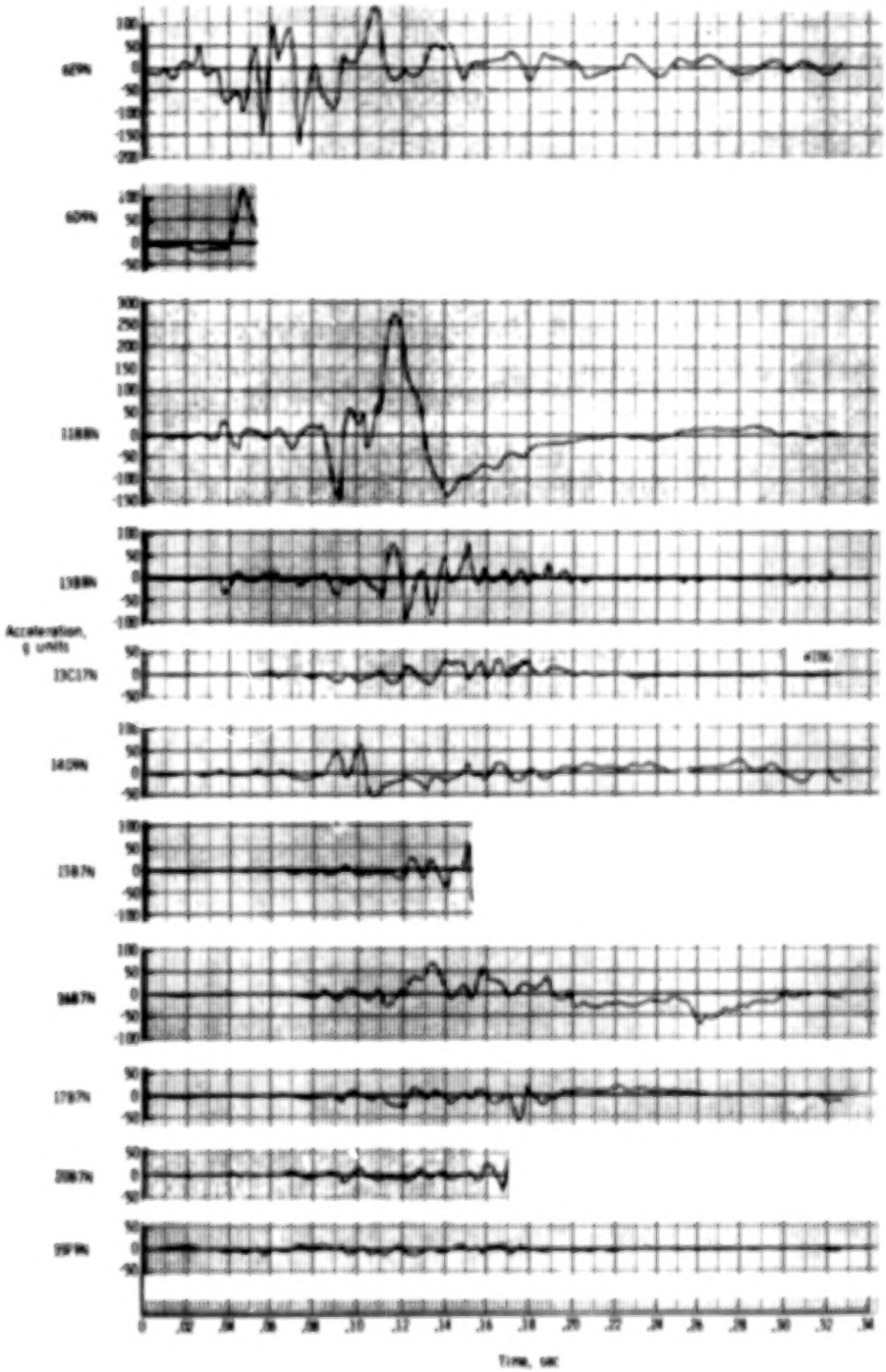

(c) Remaining normal structural accelerations.

Figure A4.- Continued.

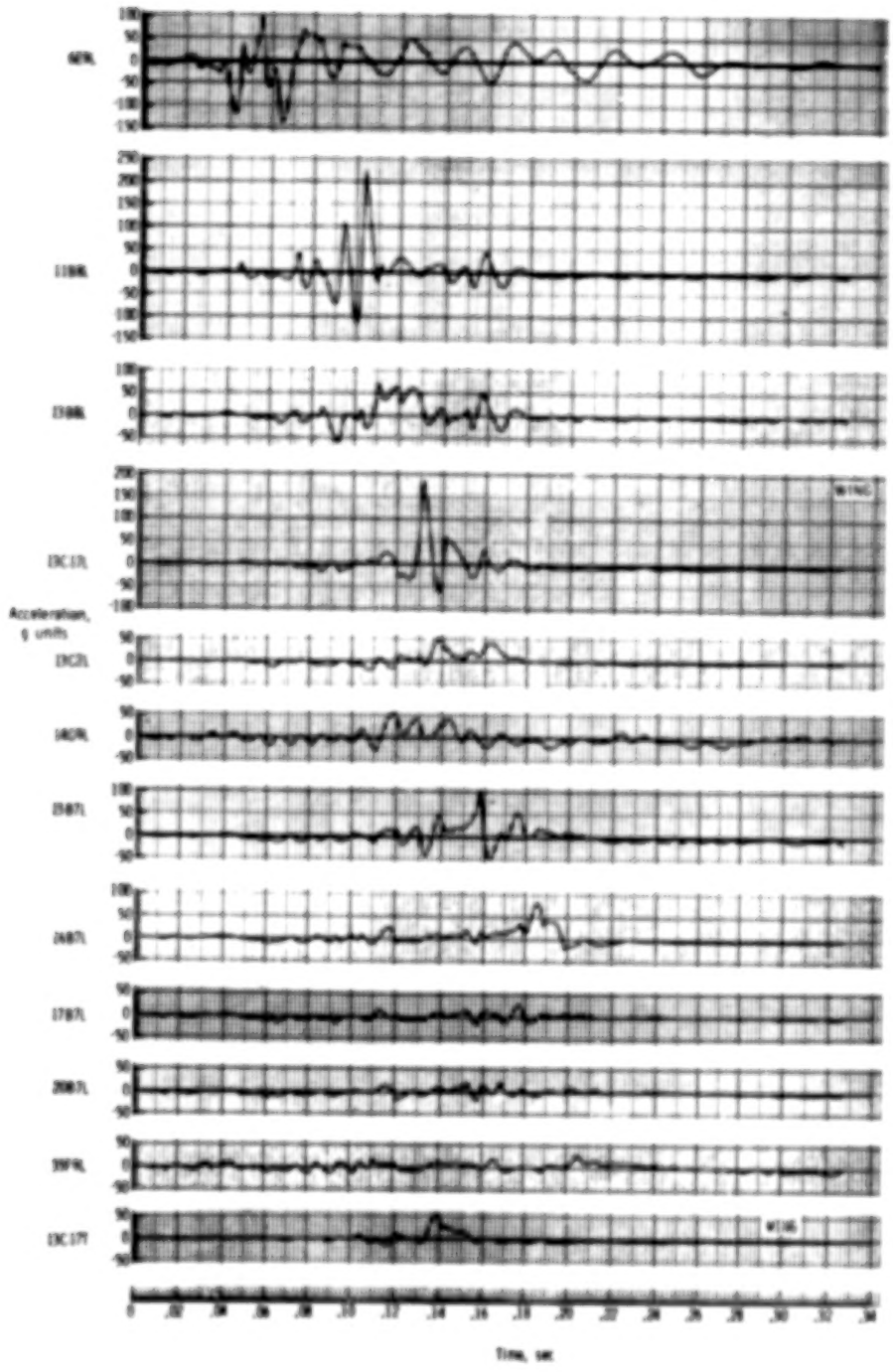

(d) Remaining longitudinal structural accelerations.

Figure A4.- Continued.

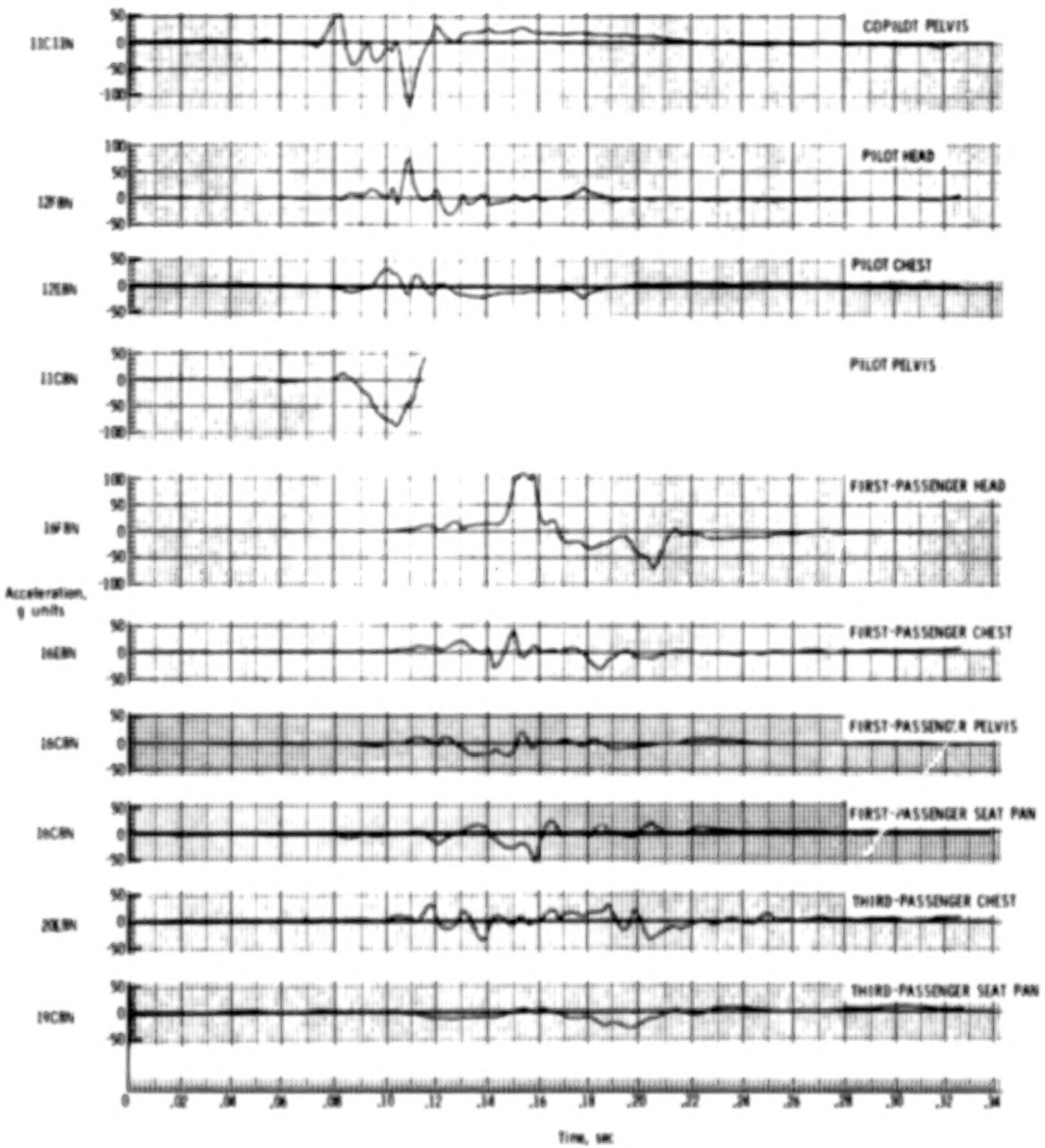

(e) Normal accelerations in dummies and on seats.

Figure A4.- Continued.

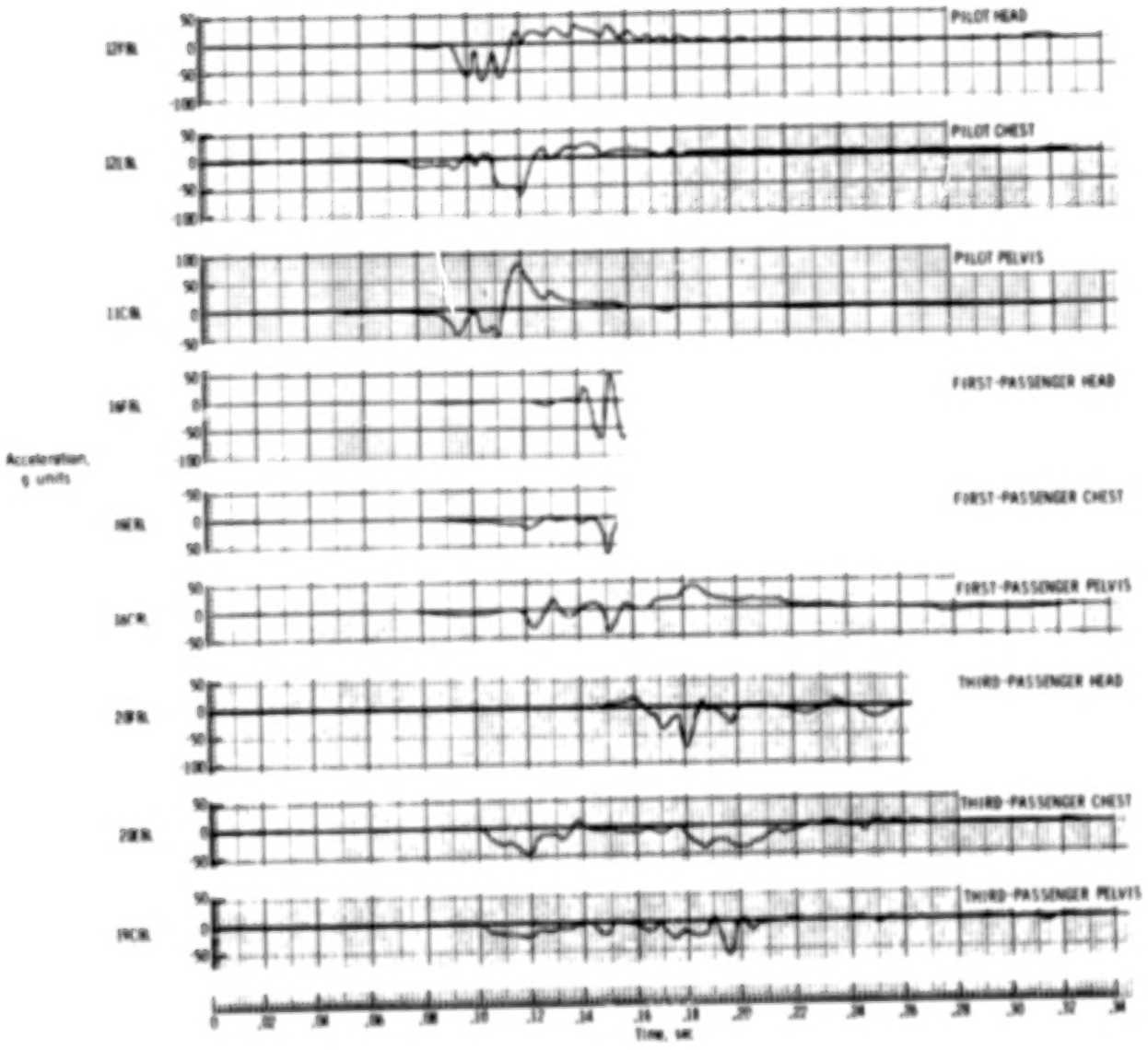

(f) Longitudinal accelerations in dummies.

Figure A4.- Concluded.

A motion-picture film supplement L-1247 is available on loan. Requests will be filled in the order received. You will be notified of the approximate date scheduled.

The film (16 mm, 11 min, color, silent) shows various views of three general-aviation airplane specimens at 24, 400, and 2000 pps for three flight-path angles during the impact sequence.

Requests for the film should be addressed to:

NASA Langley Research Center
Att: Photographic Branch, Mail Stop 425
Hampton, VA 23665

CUT

Date _____

Please send, on loan, copy of film supplement L-1247 to NASA TP-1210.

_____
Name of organization

_____
Street number

_____
City and State Zip code

Attention: Mr. _____

CUT

Place
Stamp
Here

NASA Langley Research Center
Att: Photographic Branch, Mail Stop 425
Hampton, VA 23665

1. Report No.	2. Government Accession No.	3. Recipient's Catalog No.
NASA TP-1210		

4. Title and Subtitle	5. Report Date
LIGHT AIRPLANE CRASH TESTS AT THREE FLIGHT-PATH ANGLES	June 1978
	6. Performing Organization Code
7. Author(s)	8. Performing Organization Report No.
Claude B. Castle and Emilio Alfaro-Bou	L-12060
	10. Work Unit No.
9. Performing Organization Name and Address	505-02-33-02
NASA Langley Research Center Hampton, VA 23665	11. Contract or Grant No.
	13. Type of Report and Period Covered
12. Sponsoring Agency Name and Address	Technical Paper
National Aeronautics and Space Administration Washington, DC 20546	14. Sponsoring Agency Code

15. Supplementary Notes

Technical Film Supplement L-1247 available on request.

16. Abstract

Three similar twin-engine general-aviation airplane specimens were crash tested at the Langley impact dynamics research facility at 27 m/sec and at flight-path angles of -15°, -30°, and -45°. Other flight parameters were held constant. The test facility, instrumentation, test specimens, and test method are briefly described. Structural damage and accelerometer data for each of the three impact conditions are presented and discussed.

17. Key Words (Suggested by Author(s))	18. Distribution Statement
Crash worthiness Airplane crash tests Crash damage	Unclassified - Unlimited Subject Category 39

19. Security Classif. (of this report)	20. Security Classif. (of this page)	21. No. of Pages	22. Price*
Unclassified	Unclassified	67	$5.25

* For sale by the National Technical Information Service, Springfield, Virginia 22161

NASA-Langley, 1978